Cell Chemical Biology

A covalent inhibitor targeting Cys16 on RhoA in colorectal cancer

Graphical abstract

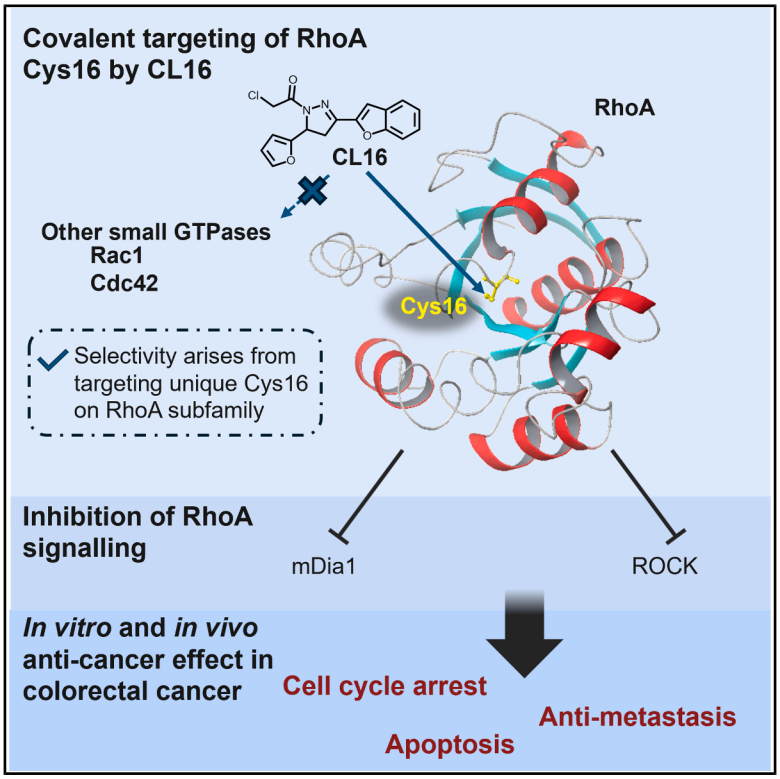

Highlights

- ABPP screening on RhoA, Cdc42, and Rac1 discovers CL16 targeting RhoA Cys16
- RhoA Cys16 is a good targetable site for specific and functional binding
- CL16 inhibits RhoA and mediates anticancer effects in colorectal cancers (CRC)
- CL16 demonstrates antitumor effects in mouse CRC models with no observable toxicity

Authors

Tin-Yan Koo, Jason Ying Ki Li, Nga-Sze Lee, ..., Stephanie Ma, Jingying Zhou, Clive Yik-Sham Chung

Correspondence

cyschung@hku.hk

In brief

RhoA is a cancer target in colorectal cancer (CRC) but remains undrugged. Koo et al. identified CL16, which covalently targets the unique Cys16 on RhoA subfamily. CL16 binding effectively inhibits RhoA protein, resulting in promising anticancer and anti-metastatic effects. This study highlights RhoA Cys16 as a targetable hotspot for CRC treatment.

Koo et al., 2025, Cell Chemical Biology *32*, 1150–1165
September 18, 2025 © 2025 The Authors. Published by Elsevier Ltd.
https://doi.org/10.1016/j.chembiol.2025.08.004

CellPress

CellPress
OPEN ACCESS

Cell Chemical Biology

Article

A covalent inhibitor targeting Cys16 on RhoA in colorectal cancer

Tin-Yan Koo,[1,9] Jason Ying Ki Li,[1,9] Nga-Sze Lee,[1,9] Jintian Chen,[2] Hillary Yui-Yan Yip,[1] Ianto Bosheng Huang,[1,3] Kai-Yu Ng,[1,3] Helen H.N. Yan,[4,5] Suet Yi Leung,[4,5,6] Stephanie Ma,[1,3,7,8] Jingying Zhou,[2] and Clive Yik-Sham Chung[1,4,5,8,10,*]

[1]School of Biomedical Sciences, Li Ka Shing Faculty of Medicine, The University of Hong Kong, Hong Kong SAR, China
[2]School of Biomedical Sciences, The Chinese University of Hong Kong, Hong Kong SAR, China
[3]Laboratory for Synthetic Chemistry and Chemical Biology, Health@InnoHK, Hong Kong Science Park, Hong Kong, China
[4]Department of Pathology, School of Clinical Medicine, Li Ka Shing Faculty of Medicine, The University of Hong Kong, Queen Mary Hospital, Hong Kong SAR, China
[5]Centre for Oncology and Immunology, Hong Kong Science Park, Hong Kong SAR, China
[6]Centre for PanorOmic Sciences, LKS Faculty of Medicine, The University of Hong Kong, Hong Kong SAR, China
[7]The University of Hong Kong – Shenzhen Hospital, Shenzhen, China
[8]State Key Laboratory of Liver Research, The University of Hong Kong, Hong Kong SAR, China
[9]These authors contributed equally
[10]Lead contact
*Correspondence: cyschung@hku.hk
https://doi.org/10.1016/j.chembiol.2025.08.004

SIGNIFICANCE RhoA is associated closely with carcinogenesis and metastasis but was considered as "undruggable". To achieve specific RhoA targeting for treatment of colorectal cancer (CRC), we develop an activity-based protein profiling screening strategy to identify a cysteine-reactive covalent ligand, CL16, which covalently targets the unique Cys16 on RhoA-subfamily over other structurally similar Rho GTPases. Cys16 is adjacent to the functional domains of RhoA, thus covalent binding by CL16 results in the inhibition of RhoA activity and hence promising anticancer and anti-metastatic effects in CRC cells as well as in mouse CRC models with no observable toxicity. Our work should establish CL16 as a specific RhoA covalent inhibitor and presages RhoA Cys16 as a good targetable hotspot for CRC treatment.

SUMMARY

RhoA is a key cancer driver and potential colorectal cancer (CRC) therapy target but remains undrugged clinically. Using activity-based protein profiling (ABPP) and mass spectrometry (MS), we identified CL16, a covalent inhibitor targeting the unique Cys16 on RhoA subfamily, which confers high specificity over other Rho family proteins. Cys16 is adjacent to the nucleotide-binding pocket and switch regions, which are critical for RhoA function. The binding by CL16 effectively disrupts GTP binding and inhibits RhoA activity in CRC cells, leading to cytotoxic killing of CRC cells through cell-cycle arrest and apoptosis. In mouse CRC models, CL16 exhibits strong antitumor and antimetastatic effects, promotes T cell infiltration into the tumor microenvironment, and shows no observable toxicity. Our findings suggest that covalent targeting of the druggable Cys16 on RhoA offers a promising strategy for CRC treatment, providing a foundation for developing specific RhoA inhibitors for clinical application.

INTRODUCTION

Upregulation of RhoA has been reported in a number of malignancies,[1–13] including colorectal cancer (CRC)[12,13] which is the second deathliest and the third most common cancer worldwide.[14–16] RhoA governs cellular structure by interplaying with downstream effectors like mDia1 and ROCK.[17–19] Studies have shown that RhoA contributes to both ameboid and mesenchymal mobility[20,21] in 3D migration and invasion[19] indicating its importance in cancers to infiltrate nearby tissues and escape anoikis using the Rho/ROCK pathway.[6,22] In rodent models, the activation of RhoA by lysophosphatidic acid (LPA) has been found to increase tumor metastasis,[23] while silencing RhoA has been demonstrated to inhibit tumor growth.[23,24]

 © 2025 The Authors. Published by Elsevier Ltd. This is an open access article under the CC BY license (http://creativecommons.org/licenses/by/4.0/).

Additionally, oxidative stress-induced activation of RhoA/ROCK2 signaling promotes tumor growth and metastasis in human colon cancer.[25] In view of the limited efficacy in the current treatment for metastatic CRC[16] this should be advantageous for the development of drug compounds targeting RhoA which associates with CRC development and aggressiveness.[26]

Despite the therapeutic interest in RhoA, it was considered as ''undruggable'' due to its smooth surface and globular structure which make it challenging to bind with small molecules.[27,28] Attempts were made to circumvent RhoA by targeting its downstream proteins, with ROCK inhibitors Y27632[29,30] and Fasudil[31,32] as representative examples. However, ROCK inhibitors cannot completely eliminate oncogenic signals from RhoA, such as RhoA-mDia1 which mediates chromosomal instability and hence drives tumor development.[33] Therefore, the interest in targeting RhoA for cancer therapy persists, and various elegant approaches have been employed to develop RhoA inhibitors. While non-covalent RhoA inhibitors such as Rhosin are good research tools in biological studies,[27] there are only limited small animal studies to evaluate their *in vivo* antitumor activities.[34] To achieve strong binding with RhoA which has smooth surface, covalent targeting with the formation of irreversible covalent bonds should be a good strategy.[35–42] Covalent ligands[28] such as DC-Rhoin were found to target the allosteric site Cys107 of RhoA to interfere with RhoA-LARG interaction.[17,27] Yet, Cys107 is conserved in other Rho GTPases such as Rac1 and Cdc42, thus these covalent ligands are not specific toward RhoA and inhibit Rac1 and Cdc42 as well. Moreover, none of the aforementioned RhoA inhibitors have demonstrated anticancer effects in CRC models.

Targeting a unique cysteine on RhoA which is absent in Rac1 and Cdc42 should be more advantageous to achieve higher specificity and lower toxicity in treating CRC. RhoA Cys16 comes to our attention because it is the only unique cysteine on RhoA subfamily among other Rho GTPases and, more importantly, located close to the nucleotide-binding pocket and switch regions. These two domains govern RhoA activation and interactions with downstream effector proteins, respectively. Covalent targeting of Cys16 should be a promising strategy to abolish hyperactivity of RhoA in CRC without altering Rac1 and Cdc42 signals, thus allowing effective CRC treatment.

Activity-based protein profiling (ABPP) is a widely used chemoproteomics platform in covalent drug research and target identification.[43–53] In this work, we develop an ABPP screening platform to first identify cysteine-reactive compounds with strong binding onto RhoA *in vitro*, followed by a second screen on Rac1 and Cdc42 proteins. This enables us to discover lead compounds with specificity toward RhoA over Rac1 and Cdc42, as well as good potential for targeting RhoA Cys16 as it is the only unique cysteine among the three structurally similar Rho GTPases. By LC-MS/MS experiment, we confirm that CL16 binds covalently onto Cys16 of RhoA in CRC cells. This prohibits nucleotide exchange and inhibits RhoA activity in CRC cells, leading to promising anti-cancer and anti-metastatic effects in both 2D and 3D cell culture models as well as in mouse xenograft and orthotopic CRC models. Our study should provide insights into RhoA Cys16 as a druggable hotspot for cancer therapy and facilitate the development of potent and specific RhoA covalent inhibitors for treating CRCs.

RESULTS

Expressions of RhoA, GEFs, and GAPs correlate with CRC development and/or patient survival

RhoA is known to be a molecular switch governing cytoskeleton organization and cell movement, thus closely associated with cancer invasion and metastasis. It shuffles between the active GTP-bound and inactive GDP-bound states with the help of guanine exchange factors (GEFs) and GTPase activating proteins (GAPs) (Figure 1A). Therefore, the cellular activity of RhoA is not solely dependent on its expression level but rather on the crucial level of the active GTP-bound form of RhoA.

We found higher RhoA expression in tumor tissues of colon adenocarcinoma (COAD) and rectum adenocarcinoma (READ) patients compared to normal tissues (Figure 1B). Although RhoA expression did not correlate with patient survival (Figure S1), higher ARHGEF25 and AKAP13[54] expressions were associated with poor survival (Figure 1C), while lower GAP levels (ARHGAP26 and ARHGAP35) favored patient survival (Figure 1D). We also observed increases in levels of ARHGEF23 and AKAP13 (a RhoA-specific GEF with no activity on Cdc42, Rac, and Ras) with more advanced tumor stage in the COAD and READ patients (Figure 1E). In addition, CRC patients with stage IV tumors are more enriched in RhoA signaling pathway than patients with early-stage tumors (Figure 1F), indicating higher RhoA activity in advanced tumors. Together with the enrichment of Rho pathway in CRC patients with higher metastatic potential as indicated by high epithelial-mesenchymal transition (EMT) score (Figure 1G)[55] these suggest the correlation between RhoA activity and CRC development and CRC malignancy.

Gel-based ABPP experiment to identify lead compounds targeting RhoA Cys16

ABPP is known to be a powerful platform for covalent ligand screening.[43–52] We performed competitive gel-based ABPP experiment on purified human recombinant RhoA protein for the first screening and on Rac1 and Cdc42 for the second screening to identify lead compounds with specific binding onto RhoA Cys16 (Figure 2). In this experiment, the purified protein was pre-treated with in-house library of cysteine-reactive compounds or DMSO control, followed by incubation with iodoacetamide-rhodamine for cysteine-labeling. The reaction mixture was then resolved by SDS-PAGE and in-gel fluorescence was imaged. Compound-protein binding was identified by the abolition in fluorescent signals or shifts in protein bands due to covalent modifications, while silver staining was to eliminate false positives due to protein precipitation. Since the Rho GTPases share alike structures with Cys16 being the only unique cysteine on RhoA (Figure 2A), compounds showing bindings with RhoA but not Rac1 and Cdc42 should target RhoA Cys16 (Figure 2B).

In the first screening experiment with RhoA protein (Figures 2C and S2A), 6 lead compounds were found (labeled in red in Figure 2D). Dose-dependent experiments revealed strong binding affinities of CL16, CL25, CL68, and CL179 toward RhoA, with notable IC_{50} of the competitive binding from CL16 down to 440 nM (Figures 2E and S2B). In the second screening

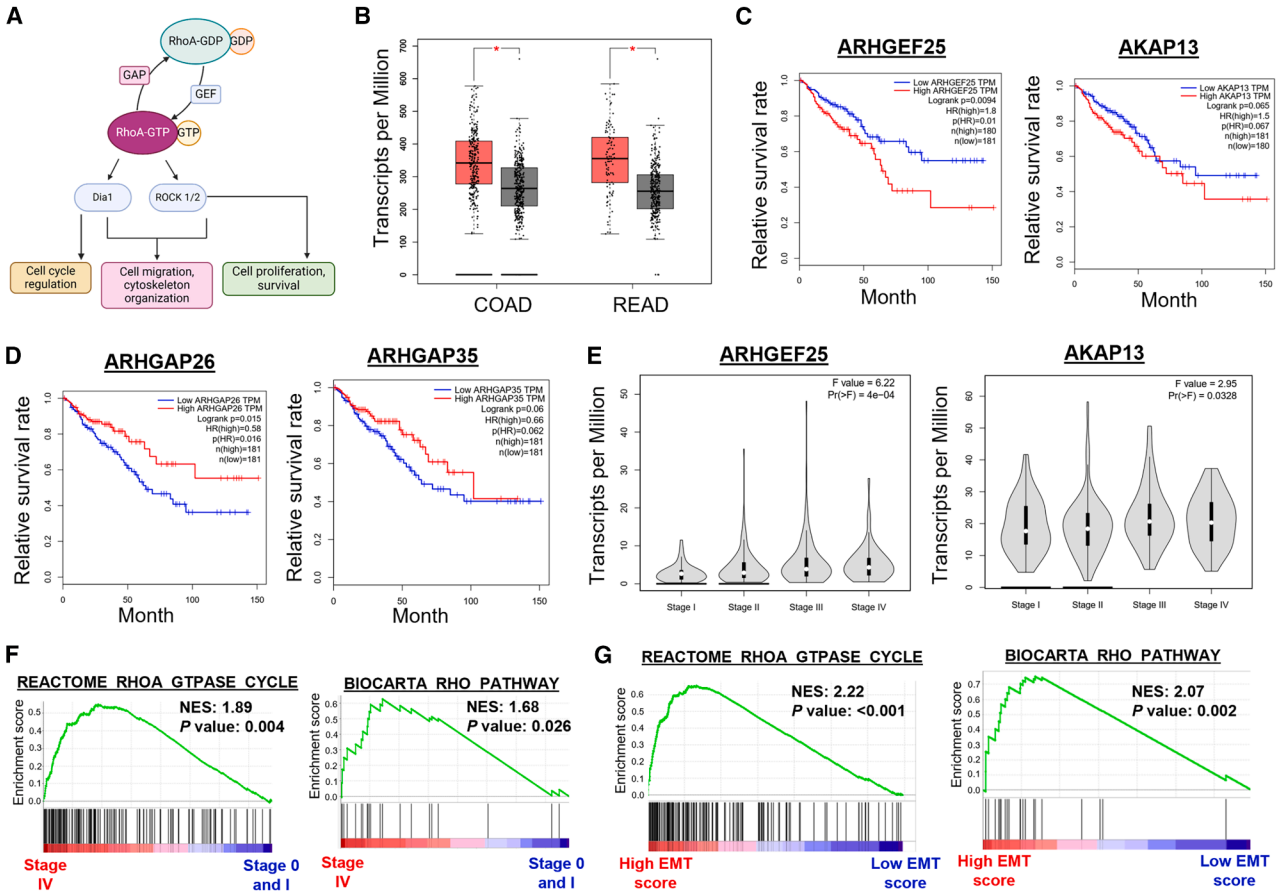

Figure 1. Expressions of RhoA, GEFs, and GAPs correlate with the colorectal cancer development and patient survival

(A) Schematic cartoon illustrating RhoA biology and its regulation by guanine exchange factors (GEFs) and GTPase activating proteins (GAPs).

(B) Analysis of RhoA expression in tumor (red) and normal tissues (gray) in patients from the colon adenocarcinoma (COAD) and rectum adenocarcinoma (READ) dataset in The Cancer Genome Atlas (TCGA) and Genotype-Tissue Expression (GTEx).

(C and D) Analysis of the expressions of GEFs and GAPs and their correlations with survival rates of patients in TCGA and GTEx.

(E) Analysis of expression of GEFs in different tumor stages of patients in TCGA and GTEx.

(F) Gene set enrichment analysis (GESA) of RhoA-related pathway in COAD and READ patients with early stage (0 and I) and late stage (IV) tumors in TCGA. NES, normalized enrichment score.

(G) GESA of RhoA-related pathway in COAD and READ patients in TCGA with high epithelial mesenchymal transition (EMT) score (mesenchymal-like) and low EMT score (epithelial-like).

experiment, CL16 showed no observable binding with Rac1 and Cdc42 (Figure 2F), while other lead compounds showed cross-reactivity at high concentrations (Figure S2C). We also found a good biostability of CL16 under physiologically relevant conditions, as revealed by the half-life of >1,000 min in PBS solution containing glutathione (GSH) and >50% of CL16 remaining intact in PBS solution with FBS after incubation for 48 h (Figure S3A). Hence, CL16 was identified and selected for further investigations regarding its binding with RhoA.

Covalent targeting of RhoA Cys16 by CL16 perturbed GTP binding onto RhoA and RhoA-GEF interactions

To confirm the covalent binding of CL16 onto RhoA Cys16 in CRC cells, a liquid chromatography coupled to tandem mass spectrometry (LC-MS/MS) experiment was conducted on colorectal cancer HCT116 cells treated with CL16. A covalent modification of RhoA Cys16 by CL16 was found (Figure 3A and Data S1), thus can explain the high specificity of CL16 for RhoA over other Rho GTPases.

As Cys16 on RhoA is adjacent to the functional domains (Figure S3B), this prompted us to study structural features of RhoA-CL16 binding to get insights into functions of this binding. Covalent docking of CL16 and RhoA (PDB: 1FTN) revealed π-π stacking, π-cation, and hydrogen bonding interactions of CL16 with Thr19, Cys20, Phe30, and Lys118 in the nucleotide-binding pocket, as well as π-cation interactions with the Mg^{2+} cofactor ion (Figures S3C and S3D). Although Rho GTPases generally bind strongly with GTP, there has been documented that covalent inhibitor could compete with GTP binding onto a recombinant KRAS GTPase[56] implying the feasibility of CL16 interfering GTP loading. This is supported by the fluorescence assay on MANT-GTP binding onto RhoA, where pre-incubation of RhoA with CL16 significantly slowed down the increase in fluorescence intensity, indicating that the

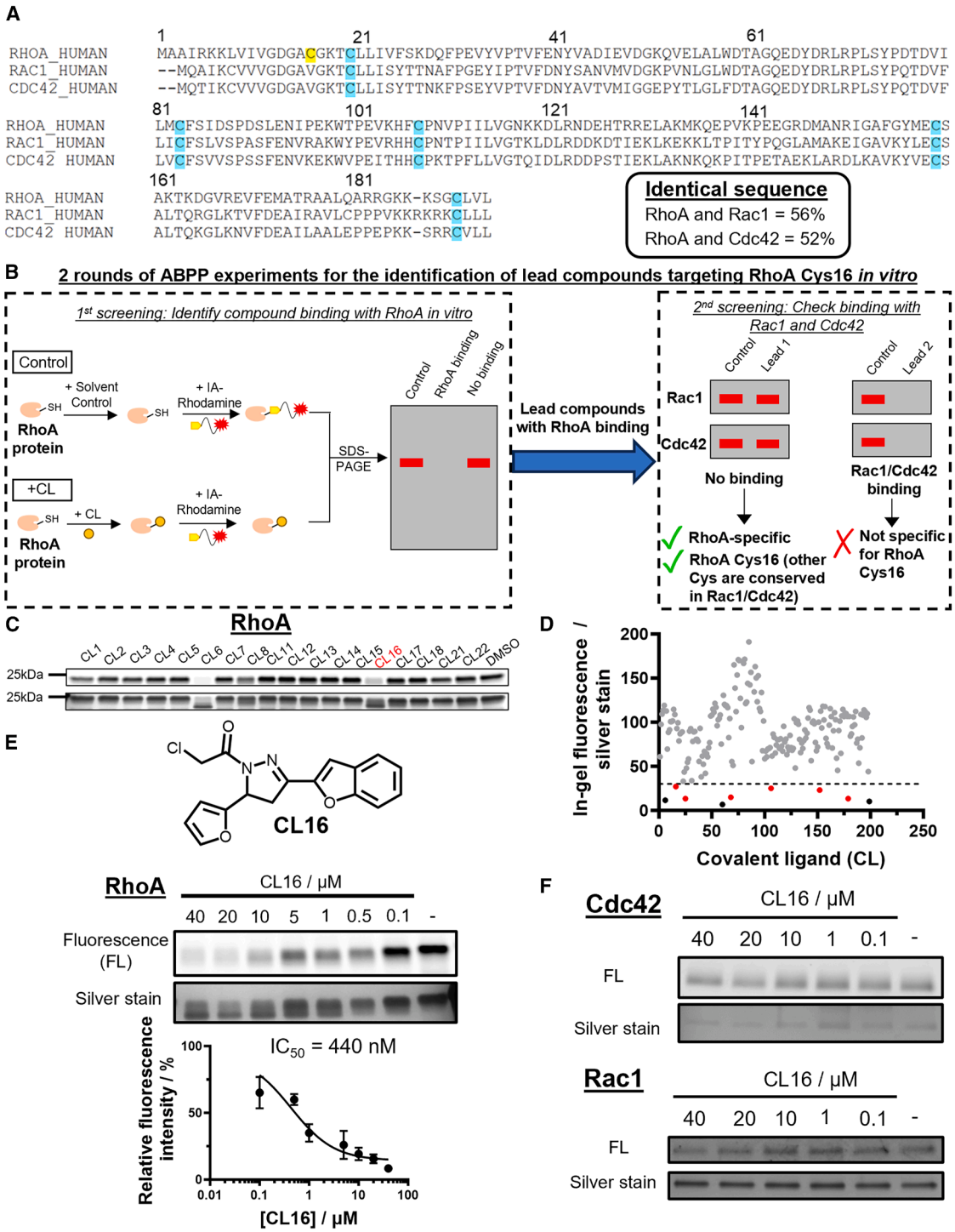

Figure 2. Activity-based protein profiling experiments to identify RhoA-specific binders

(A) Amino acid sequence alignment of human RhoA, Rac1, and Cdc42. Cys16 on RhoA is highlighted in yellow, while other conserved cysteines are highlighted in blue.

(B) Schematic cartoon illustrating the working principle of 2 rounds of activity-based protein profiling (ABPP) for screening out covalent ligands targeting RhoA Cys16 *in vitro*.

(C) Representative images of the 1st screening experiment on RhoA (top: in-gel fluorescence; bottom: silver stain). All the gel images can be found in Figure S2A.

(D) Analysis of the 1st screening result. Covalent ligands, that show lower than 30% of the intensity ratio and retain at least 70% intensity in the silver stain as compared to the DMSO control, are labeled in red and considered as lead compounds.

(E) Dose-dependent experiments to investigate CL16 binding with RhoA *in vitro*.

(F) 2nd screening experiment of CL16 with other Rho family proteins, Rac1 and Cdc42. Quantified data in (E) were shown on average ± SD from 3 different replicates/group.

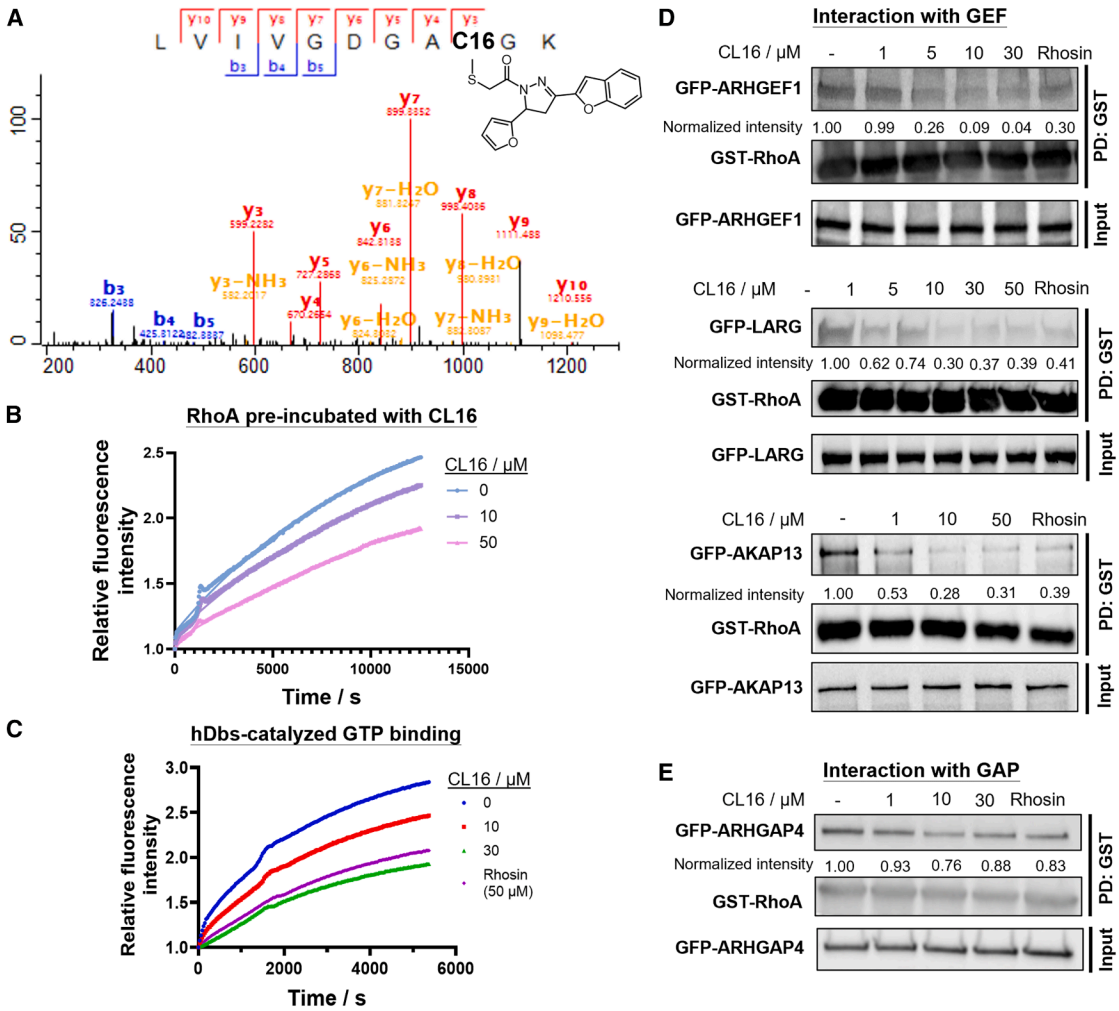

Figure 3. CL16 binding with RhoA Cys16 prohibits RhoA-GTP binding and RhoA-GEF interactions

(A) LC-MS/MS analysis on CL16-treated HCT116 cells revealed a covalent modification of RhoA Cys16 by CL16.

(B) GTP-binding assay of RhoA (0.75 μg), CL16, and GTP-MANT (5.6 μM) in the buffer solution (20 mM Tris, 50 mM NaCl, 10 mM $MgCl_2$, pH 7.5).

(C) hDbs-catalyzed GTP-binding assay of RhoA (0.75 μg), CL16, and GTP-MANT (5.6 μM) in the buffer solution.

(D and E) Co-immunoprecipitation of a mixture of CL16/Rhosin (30 μM)-treated human GST-RhoA protein (10 μg) and HEK293T cell lysates with overexpression of GFP-ARHGEF1, GFP-LARG, GFP-AKAP13, or GFP-ARHGAP4. Error bars were not shown in (B) and (C) for figure clarity. All the data in the replicate experiments can be found in the Source Data.

CL16 binding prohibited GTP loading onto RhoA (Figure 3B). Gel-based ABPP experiments revealed competitive RhoA binding between CL16 and GDP, while reduced competition was observed in the experiment with mutated RhoA T19N protein which has reduced nucleotide-binding affinity (Figure S3E). CL16 also demonstrated a stronger binding to RhoA in the presence of Mg^{2+} (Figure S3F). In addition, fluorescence-based assay showed a significant decrease in the kinetics of Dbs-mediated GTP binding onto RhoA (Figure 3C). Co-immunoprecipitation experiments revealed the disruption of RhoA interactions with GEFs or GAPs with increasing concentrations of CL16 (Figures 3D and 3E), while addition of EDTA abolished the effects of CL16 (Figure S3G), supporting the crucial interaction between Mg^{2+} and CL16 for RhoA binding. All these results illustrate that covalent targeting of Cys16 on RhoA should be a promising strategy to prohibit GTP loading onto RhoA and disrupt its interactions with effector proteins for activation and signal transduction.

Inhibition of RhoA activity in CRC cells after CL16 treatment

We next sought to examine effects of CL16 on RhoA biology in CRC cells. We investigated the activation of RhoA by FBS stimulation in serum-depleted HCT116 cells. CL16 treatment led to much lower cellular RhoA-GTP levels after serum stimulation as compared to the solvent control which showed an increase in RhoA-GTP level in the serum-re-stimulated cells. CL16 was also found to be more effective than Rhosin on inhibition of RhoA activity, as revealed by the lower RhoA-GTP level in cells treated with 10 μM of CL16 than those treated with 30 μM of Rhosin (Figure 4A).

We also examined effects of CL16 on RhoA downstream signals in CRCs. HCT116 cells incubated with solvent control

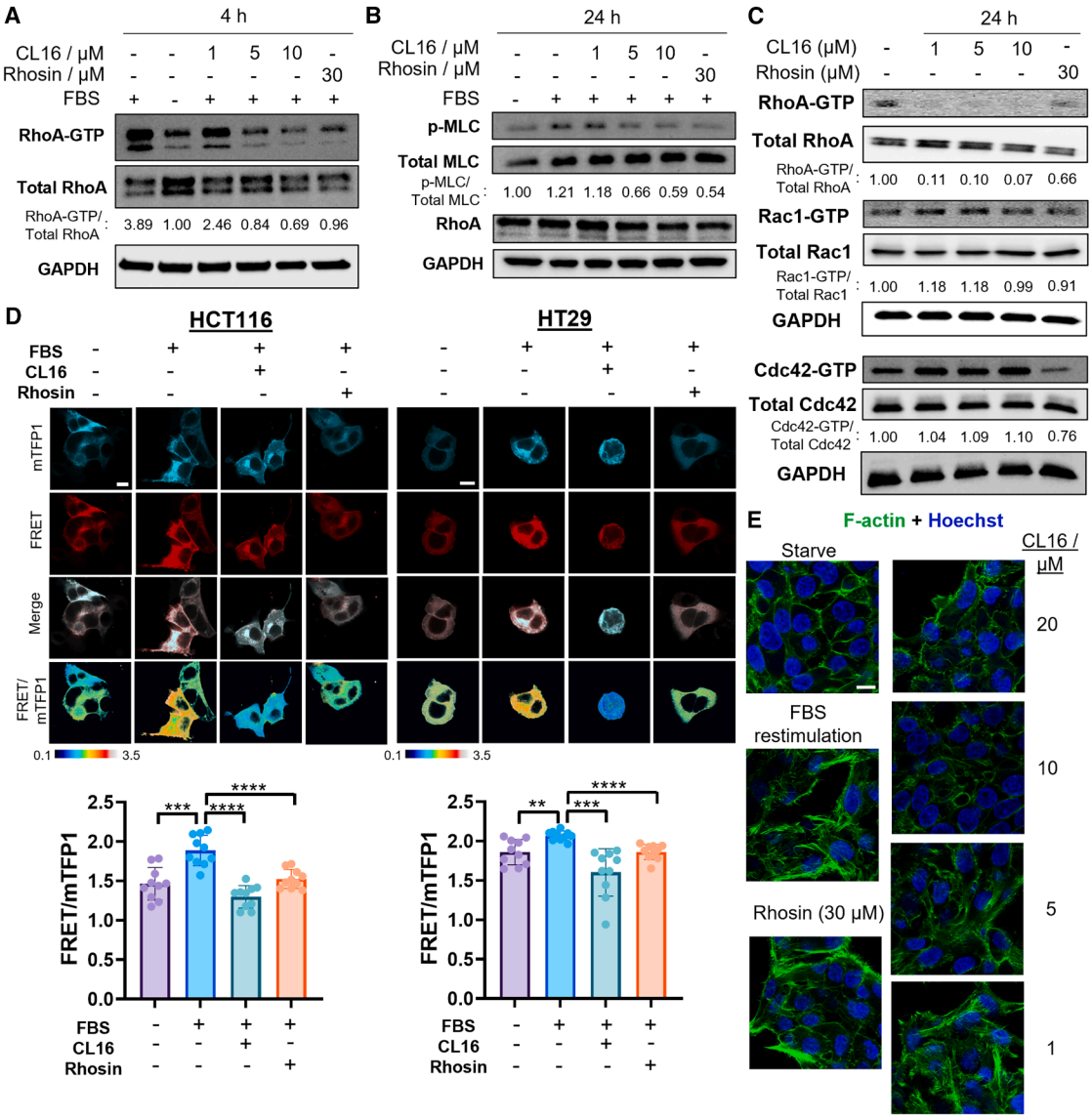

Figure 4. CL16 inhibits RhoA activity in CRC

(A) HCT116 cells were treated with solvent vehicle, CL16, or Rhosin in serum-free medium for 24 h, followed by stimulation with 10% FBS for 10 min. The cells were then lysed and subjected to rhotekin pull-down and immunoblotting.

(B) Immunoblotting to investigate phosphorylation levels of RhoA downstream protein, myosin light chain (MLC), in HCT116 cells in the serum starvation-re-stimulation experiments.

(C) HCT116 cells were incubated with solvent vehicle, CL16, or Rhosin in complete medium for 24 h. RhoA-GTP, Rac1-GTP, and Cdc42-GTP were enriched by rhotekin or PAK-PBD pull-down and determined by immunoblotting.

(D) Confocal fluorescence images from HCT116 and HT29 cells expressing FRET RhoA-biosensor treated with CL16 (10 μM) or Rhosin (30 μM). Quantified data were shown on average ± SD from $n = 10$ cells from 3 different biological replicates/group.

Statistical analysis using a two-tailed Student's t test. $^{**}p < 0.01$, $^{***}p < 0.001$, and $^{****}p < 0.0001$. Scale bars, 10 μm.

(E) Confocal fluorescence images from HCT116 cells stained with Alexa Fluor 488-Phalloidin in PBS (1:20, v/v) and Hoechst (8.2 μM). Scale bars, 10 μm.

showed elevated levels of phosphorylated myosin light chain (MLC), which is a downstream effector of RhoA, upon serum re-stimulation (Figure 4B). CL16 treatment significantly abolished the increase in phosphorylation of MLC induced by serum re-stimulation, in consistent with the promising effect of CL16 on lowering RhoA-GTP levels (Figure 4A). We observed a specific inhibition of RhoA activity in HT29 cells treated with CL16 with no significant changes in the activity of other Rho GTPases such as Rac1 and Cdc42, while Rhosin inhibited Cdc42 in HT29 cells at its working concentration for RhoA inhibition (30 μM, Figure 4C). Over 85% of HT29 cells remained viable after 4 h treatment with 10 μM of CL16 (Figure S4A), ruling out the decrease in RhoA-GTP levels due to cytotoxic effects of the compound. No significant changes in the active RhoB-GTP and RhoC-GTP levels were found in the CL16-treated HT29 cells (Figures S4B and S4C),

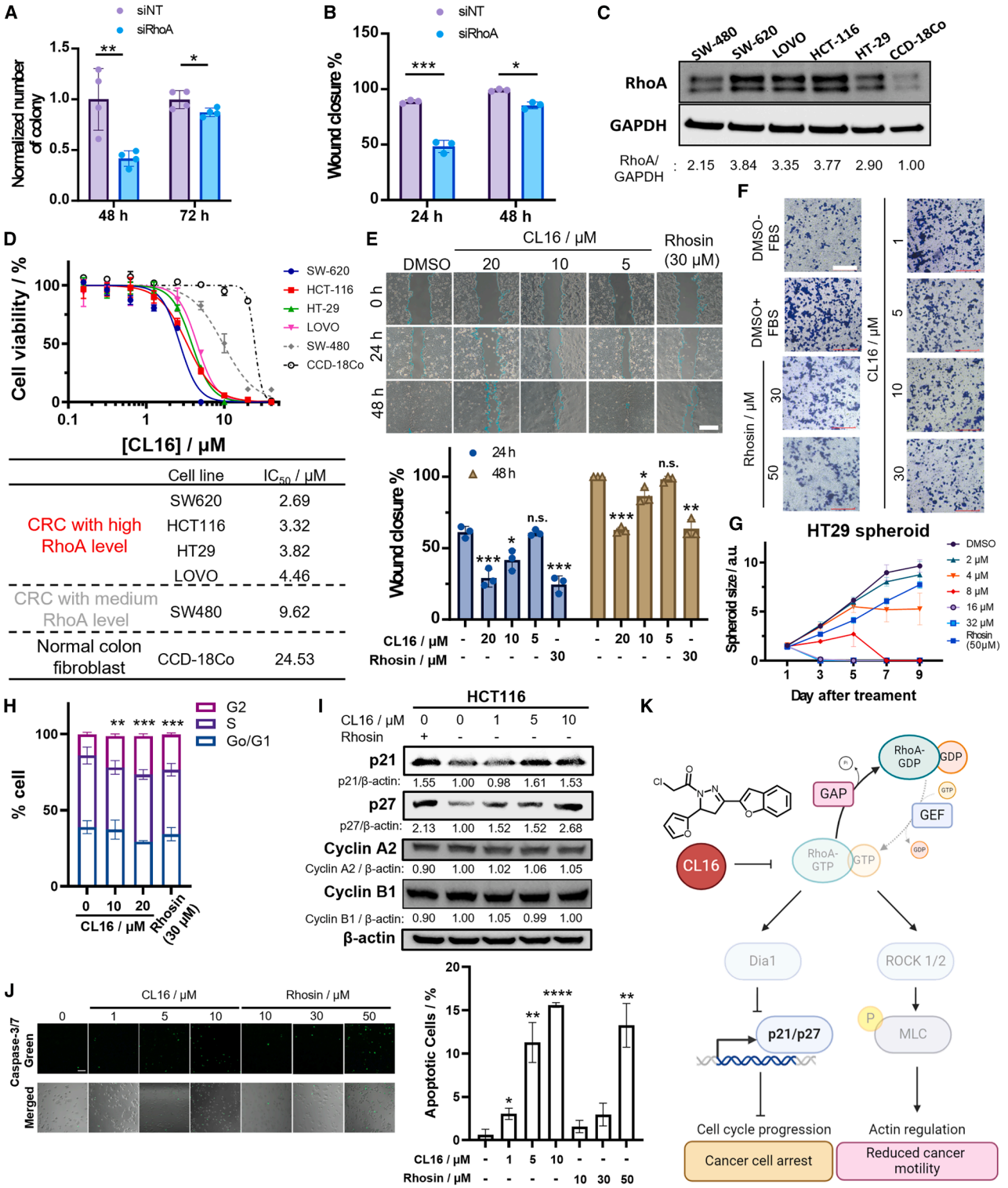

	Cell line	IC_{50} / μM
CRC with high RhoA level	SW620	2.69
	HCT116	3.32
	HT29	3.82
	LOVO	4.46
CRC with medium RhoA level	SW480	9.62
Normal colon fibroblast	CCD-18Co	24.53

Figure 5. Anticancer and antimetastatic effects on CRC through RhoA downregulation

(A and B) Colony formation and cell migration assays on HT29 cells with non-targeting (NT) or RhoA knockdown by siRNA.

(C) Immunoblotting of RhoA in CRC and normal colon fibroblast, CCD-18Co.

(D) MTT assay to determine cell viability of CRCs and normal colon fibroblast CCD-18Co cells treated with CL16 for 48 h (n = 3).

(E) Wound healing assay on HT29 cells incubated with solvent vehicle, CL16, or Rhosin (n = 3).

(F) Transwell invasion assay on HT29 cells treated with CL16 or Rhosin for 24 h.

(legend continued on next page)

highlighting the specificity of RhoA inhibition by CL16 in CRC cells.

To further validate the inhibitory effects of CL16 on RhoA, we transfected HCT116 and HT29 cells, respectively, with a FRET-RhoA biosensor where cells with elevated RhoA activity will show a higher FRET/mTFP1 ratio.[57,58] CL16 treatment abolished the increases in FRET/mTFP1 from both the transfected HCT116 and HT29 cells with serum re-stimulation (Figure 4D). In addition, we observed a reduction of F-actin fibers in cells treated with CL16 in the serum re-stimulation experiment, as compared to the solvent control (Figure 4E). Since RhoA is known to regulate cytoskeletal dynamics and its activation can induce the formation of contractile F-actin,[19,27,28] the reduction of F-actin fibers by CL16 treatment supports the inhibitory roles of CL16 on RhoA signaling.

Anticancer and anti-metastatic effects from CL16 on CRC through RhoA inhibition

Overexpression of RhoA has been observed in tumor tissues of CRC patients (Figure 1B), and its hyperactivity has been associated with poor prognosis and aggressive behaviors of CRCs, as reported in literature[59,60] and found in our analysis of The Cancer Genome Atlas (TCGA) and Genotype-Tissue Expression (GTEx) datasets (Figures 1B–1F). With the promising RhoA inhibitory effects from CL16, this initiated us to explore anti-cancer and anti-metastatic properties of CL16 in CRCs. We first confirmed that genetic knockdown of RhoA, but not RhoB and RhoC, by siRNAs slowed down colony formation and migration of CRCs (Figures 5A and 5B and S4D–S4I). We also found a much lower expression level of RhoA in normal colon fibroblast CCD-18Co cells, as compared to CRCs, inversely relating to the cytotoxic IC_{50} of CL16 (Figures 5C and 5D). This indicates a good therapeutic window for using CL16 to treat CRCs, especially those with higher RhoA activity (Figures 5D and S4J). In addition, CL16 showed good efficacy in reducing HT29 cell motility, as shown in the wound healing assay (Figure 5E) and transwell invasion assay (Figure 5F). To further investigate the anticancer effects of CL16, HT29 and metastatic SW620 cells were inoculated as 3D spheroids in low-affinity plate. CL16 treatment resulted in significant growth inhibitions in both models and was found to be more effective than Rhosin treatment as reflected by the lower dosages of CL16 to mediate similar anticancer effects (Figure 5G and S4K–S4M). The low cytotoxic IC_{50} values of CL16 in SW620 and HT29 spheroids suggest the good penetration of CL16 through tumor mass and imply its potentials for *in vivo* applications.

Next, we investigated the molecular mechanisms of anticancer effects from CL16. Flow cytometry analysis on HCT116 and SW620 cells treated with CL16 and Rhosin revealed a significant increase in G2 phase cell population (Figures 5H and S4N). Western blotting experiments showed an increase in p21 and p27 protein levels in HCT116, HT29, and SW620 cells after CL16 treatment (Figures 5I and S4O), while no significant changes were observed in cyclin A2 and cyclin B1. CL16 treatment also mediated cell apoptosis, as found in the confocal fluorescence imaging experiment using caspase-3/7 green detection reagent (Figure 5J). The elevated levels of p21 and p27 are attributable to the downregulated RhoA-Dia1 signaling by CL16. This leads to inhibitory effects of p21 and p27 on CDK1-cyclin B complex, preventing CRC cells from progressing into mitosis and inducing G2 phase arrest that triggers apoptotic cell death (Figure 5K).

Chemical biology and chemoproteomics experiments reveal RhoA as the primary protein target of CL16 in CRC

To validate RhoA as the protein target of CL16 in CRCs, we synthesized a molecular probe of CL16, CL16-alkyne (Figure 6A), which contains an alkyne handle that allows functionalization through copper-catalyzed azide-alkyne cycloaddition (CuAAC) for studying CL16-protein binding. We first incubated HEK293T cells expressing FLAG-RhoA with CL16-alkyne, followed by anti-FLAG immunoprecipitation and then CuAAC to install fluorescent TAMRA onto the CL16-alkyne-bound proteins. A strong in-gel fluorescence band was found, and a parallel immunoblotting experiment confirmed that the in-gel fluorescence is from the FLAG-RhoA protein (Figure 6B). This illustrates the ability of CL16-alkyne to capture RhoA in live cells. Notably, pre-incubation of the HEK293T cells expressing FLAG-RhoA with CL16 revealed a significant decrease in in-gel fluorescence intensity (Figure 6B), suggesting competitive binding and hence RhoA is a protein target of CL16. All these results, together with the shared protein targets of CL16 and CL16-alkyne found in the gel-based ABPP experiment (Figure S5A), validated CL16-alkyne as a probe of CL16 for target identification. The binding of CL16 and CL16-alkyne with endogenous RhoA in CRC cells was confirmed by the treatment of HT29 cells with the compounds, followed by CuAAC to install desthiobiotin, enrichment by streptavidin beads and immunoblotting (Figure 6C).

CL16-alkyne was then employed to examine any off-target binding from CL16 in CRCs. HCT116 cells were pre-treated with solvent vehicle or CL16 for 2 h, followed by incubation with CL16-alkyne for another 2 h. The probe-labeled proteins were then installed with desthiobiotin through CuAAC, enriched, tryptic digested, and profiled by LC-MS/MS (Figures 6D and 6E and Data S2). Peptides with fold change (Control/CL16)>4 and $p < 0.05$ (i.e., at least 75% occupancy and statistical significance) were considered as targets bound with CL16. RhoA was found to be one of the protein targets of CL16 (Figure 6E) and was the only protein identified in both the LC-MS/MS experiments on CL16-treated HCT116 cells and CL16-alkyne-probed HCT116 cells (Figure 6F), suggesting that RhoA is the primary target of CL16. We also utilized CL16-alkyne to investigate the

(G) HT29 spheroid growth in the presence of solvent vehicle, CL16, or Rhosin ($n = 3$).
(H) Flow cytometry analysis of cell cycle distribution of HCT116 cells after incubation with CL16 or Rhosin for 24 h.
(I) Immunoblotting of cell cycle checkpoint proteins in HCT116 cells after treatment with CL16 or Rhosin (30 μM) for 24 h.
(J) Apoptosis assay on CL16-treated HCT116 cells using caspase-3/7 green detection reagent.
(K) Schematic cartoon illustrating the mechanism of action of CL16 to mediate anticancer and antimetastatic effects by RhoA inhibition. Quantified data were shown in average ± SD.
Statistical analysis using a two-tailed Student's t test. $^{*}p < 0.05$, $^{**}p < 0.01$, and $^{***}p < 0.001$. Scale bars, 100 μm.

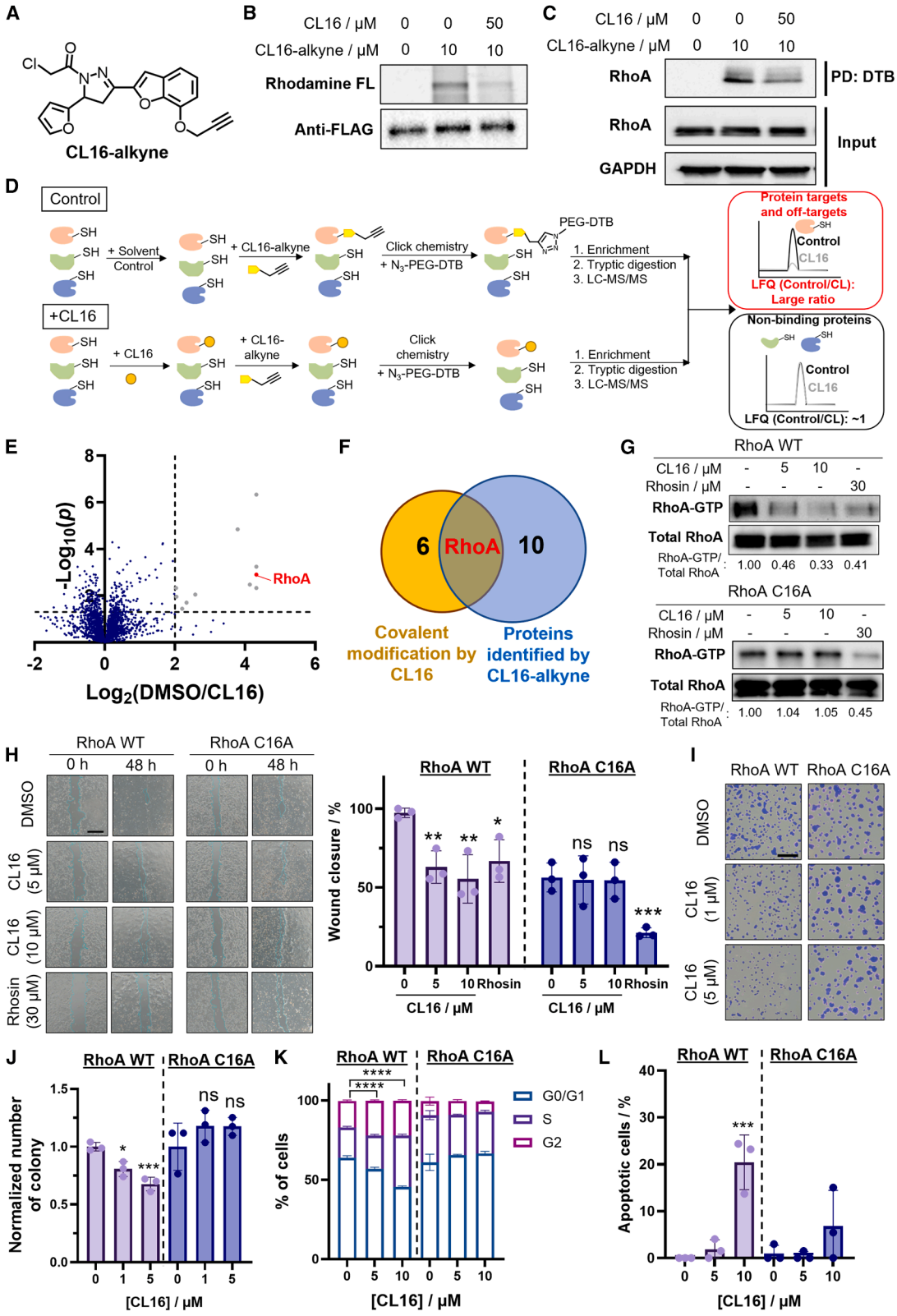

(legend on next page)

kinetics of the reaction between CL16 and RhoA protein (Figures S3H and S3I), and the maximal rate of inactivation (k_{inact}) and K_i were found to be 0.10 s^{-1} and 24.0 μM, respectively, similar to the kinetics of the reported cysteine-targeting covalent ligands.[61]

CL16 exhibits its biological activity in CRC through covalent targeting of RhoA Cys16

To validate the molecular mechanism of RhoA inhibition and anti-cancer properties from CL16, we first performed RhoA KD in HT29 cells by siRNA, and confirmed that CL16 lost its anti-proliferative effects on the RhoA KD cells (Figures S5B and S5C). Then, we studied the effects of CL16 in HT29 cells expressing RhoA WT protein and HT29 cells with RhoA C16A knock-in by CRISPR-Cas9, respectively. CL16 treatment resulted in a significant decrease in the active RhoA-GTP level in the HT29 cells, but not in the RhoA C16A mutant-expressing cells (Figure 6G). We found significant decreases in cell proliferation and migration in HT29 cells after treatment with CL16, while no inhibitory effects from CL16 were observed in mutant cells (Figures 6H–6J). The mutant cells were also rescued from CL16-induced apoptosis and G2-phase cell-cycle arrest (Figures 6K and 6L). All these results illustrate that CL16 inhibited RhoA activity and mediated anti-cancer properties in CRC primarily through covalent targeting of RhoA Cys16.

CL16 demonstrated promising *in vivo* antitumor effects on CRC

The therapeutic potentials of CL16 to treat CRC through covalent targeting and inhibition of RhoA were further investigated by small animal CRC models. In nude mice with CRC xenografts, CL16 significantly inhibited tumor growth of HCT116 xenograft, HT29 xenograft and SW620 xenograft (Figures 7 and S6), compared to vehicle control. Immunohistochemistry on tumor tissues in the treated group showed a reduction in Ki67 level (Figure 7C), indicating a decrease in cancer cell proliferation after CL16 treatment. The elevated cleaved caspase-3 level in the tumor tissues from CL16-treated mice suggested the induction of apoptosis in CRC cells (Figure 7C), highlighting the effective killing of cancer cells *in vivo* by CL16. In addition, there were no observable reductions in body weight (Figures S6D and S6E) or damages on major organs from H&E staining of treated mice (Figure 7E), suggesting minimal toxicity from CL16 treatment.

On the basis that Cys16 is conserved on mouse RhoA protein, we also examined its antitumor effects in an immunocompetent, orthotopic mouse CRC model, which was established by the inoculation of mouse CRC cells, SL4[62] intracecally (Figure S6G). Similar to the findings in human CRC, CL16 treatment significantly decreased the viability of SL4 in 2D cell culture (Figure S6M) and significantly reduced the tumor weight in the orthotopic mouse CRC model without systemic toxicity observed (Figures 7F and 7G; S6H). A downregulation of phosphorylation of MLC was found in the tumor tissues of CL16-treated mice (Figure S6N), supporting the RhoA inhibitory effects of CL16 *in vivo*. H&E staining on tumor tissues from CL16-treated mice revealed nuclear atypia such as nuclear condensation and fragmentation (Figure 7G), indicating the induction of apoptosis. This is supported by the immunohistochemistry of cleaved caspase-3, which showed an elevated level in the tumor tissues from the treated mice (Figures S6K and S6L). The decrease in Ki67 in tumor tissues was in line with the promising antitumor effects of CL16. In addition, we observed tumor metastasis to liver in the control mice, while CL16 treatment prohibited metastasis (Figures S6I and S6J). Together with the decrease in VEGFR2 level in the immunohistochemistry experiment (Figures S6K and S6L), this illustrates the anti-metastatic properties of CL16 *in vivo*. Interestingly, increases in CD3, CD4, and CD8 were found in the immunohistochemistry of the tumor tissues from the CL16-treated mice (Figure 7H), suggesting an increase in infiltration of cytotoxic T cells into the tumor microenvironment after CL16 treatment. To the best of our knowledge, this is the first reported study showing an increase in immunity through RhoA inhibition in CRC cells by a small molecule compound.

DISCUSSION

CRC remains one of the leading causes of deaths worldwide, with limited treatment options especially in the metastatic stage. RhoA is an important molecular switch that governs cytoskeleton organization and cell movement, thus closely associated with cancer invasion and metastasis. Given the complexity of RhoA regulation, measurement on the levels of active RhoA (GTP-bound RhoA) in biological samples, instead of the expression of RhoA only, should provide better insights into the functions of RhoA in CRC development. We observed higher expressions of RhoA in tumor tissues of patients with COAD and READ

Figure 6. Target identification and validation for CL16

(A) Chemical structure of the molecular probe for CL16, CL16-alkyne.

(B) Anti-FLAG immunoprecipitation of HEK293T cells expressing FLAG-RhoA pretreated with solvent vehicle or CL16 prior to CL16-alkyne treatment. The enriched proteins were reacted with azide-fluor 545 through CuAAC and separated by SDS-PAGE. The protein bands were then visualized by in-gel fluorescence or immunoblotted.

(C) HT29 cells were pre-treated with solvent vehicle or CL16 for 2 h, followed by the incubation with CL16-alkyne in complete medium for another 2 h. The cells were then lysed, and the CL16-alkyne-labeled proteins were installed with DTB by CuAAC. The labeled proteins were then enriched by streptavidin beads, followed by immunoblotting.

(D) Schematic workflow illustrating the MS experiment using CL16-alkyne for the identification of protein targets of CL16 in HCT116 cells.

(E) Volcano plot of the MS experiment on HCT116 cells probed by CL16-alkyne.

(F) Comparison of the proteins in HCT116 cells modified by CL16 (Data S1) and the proteins in HCT116 cells probed by CL16-alkyne (Data S2).

(G) HT29 cells expressing RhoA WT or C16A protein were incubated with solvent vehicle, CL16 or Rhosin in complete medium for 24 h. The cells were then washed, lysed, subjected to rhotekin pull-down, and immunoblotted.

(H–K) (H) Wound healing assay, (I and J) colony formation assay, (K) cell cycle analysis and (L) apoptosis assay on HT29 cells expressing RhoA WT or C16A protein incubated with solvent vehicle, CL16, or Rhosin in complete medium. Quantified data were shown in average ± SD (n = 3).

Statistical analysis using a two-tailed Student's t test. *p < 0.05, **p < 0.01, ***p < 0.001, and ****p < 0.0001. Scale bars, 100 μm.

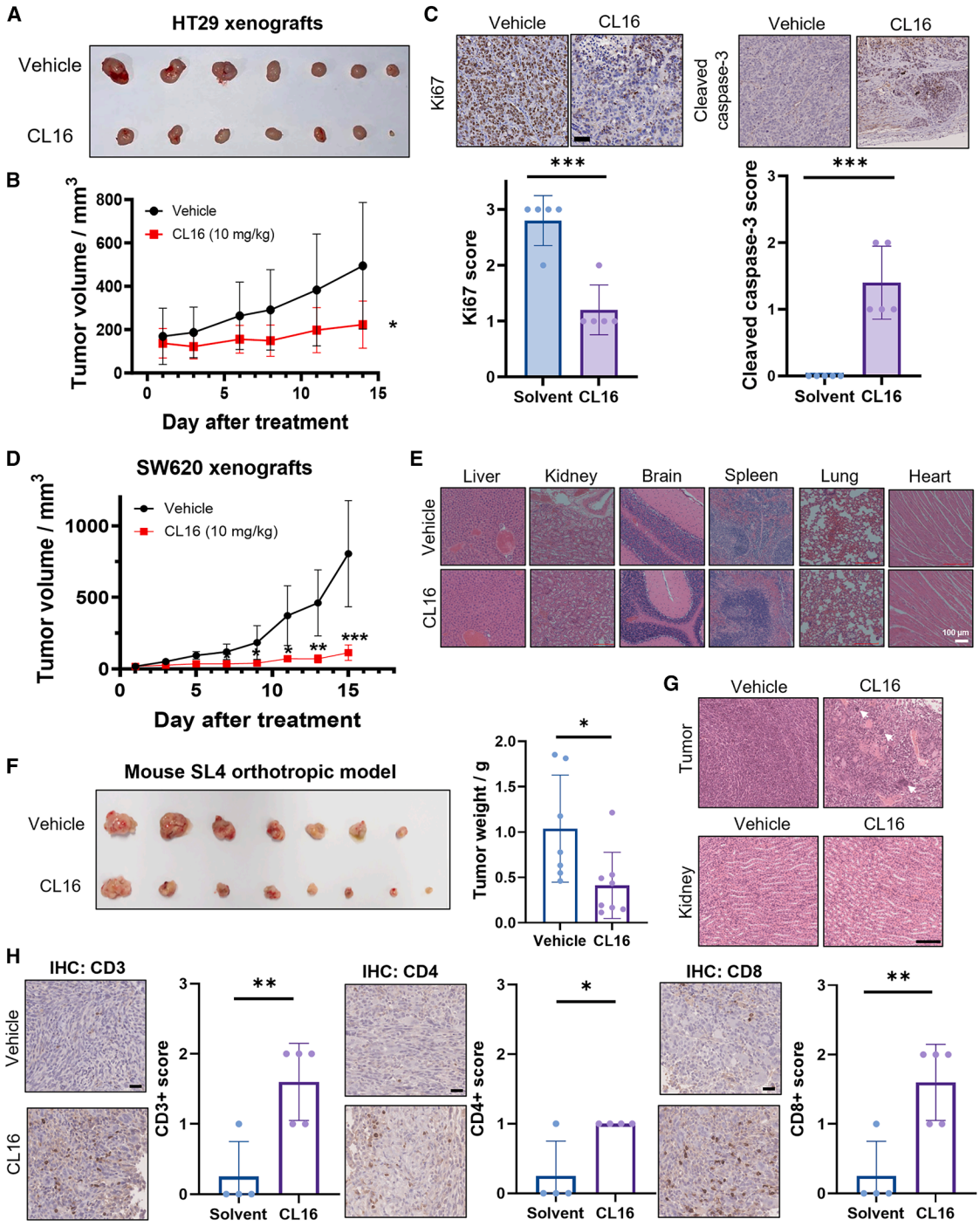

Figure 7. *In vivo* antitumor activity of CL16 in mouse CRC models

(A) Tumors harvested from mice with HT29 xenografts (n = 7) treated with solvent vehicle or CL16 through i.p. injection.

(B) Change in tumor volume in the treated mice.

(C) Immunohistochemistry of the tumor tissues from the vehicle- or CL16-treated mice, n = 5.

(D) Changes in tumor volume in mice with SW620 xenografts (n = 5) treated with solvent vehicle or CL16 through i.p. injection.

(E) H&E staining of major organ tissues from the vehicle- or CL16-treated mice with SW620 xenografts.

(F) The photo and weight of tumors from the mice with SL4 orthotopic model treated with vehicle (n = 7) or CL16 (n = 8) at the endpoint of the experiment.

(G) H&E staining of tumor and kidney tissues from the vehicle- or CL16-treated mice. The white arrows point to the nuclear atypia in the tumor tissues.

(H) Immunohistochemistry staining of CD3, CD4, and CD8 on tumor tissues from the vehicle- or CL16-treated mice. Quantified data were shown in average ± SD. Statistical analysis using a two-tailed Student's t test. *p < 0.05, **p < 0.01, and ***p < 0.001. Scale bars, 50 μm.

than normal tissues in deposited clinical dataset. A higher enrichment of genes related to RhoA pathway has been found in CRC patients with stage-IV tumors or high EMT score, illustrating the elevated RhoA activity in advanced CRC. Combined with the poor survival rates of patients with higher expressions of AKAP13 (a RhoA GTPase-specific GEF) but better survival with higher expressions of GAPs, all these analyses suggest a positive correlation between RhoA activity and CRC development/progression, and hence RhoA inhibition should be a promising strategy for CRC treatment, similar to what has been reported in the treatment of breast cancer.[27,28]

Since RhoA mutation is not frequently found in CRC patient,[63] a pan-RhoA inhibitor should be effective in inhibiting RhoA hyperactivity in CRC. The development of promising RhoA inhibitors is still challenging due to the lack of good binding pockets in RhoA, and hence RhoA was once considered "undruggable". Rhosin and DC-Rhoin are two successful compounds that could bind and inhibit the "undruggable" RhoA. Yet, there were limited studies on the *in vivo* anticancer properties of Rhosin in small animals. The inhibition of Rac1 by DC-Rhoin can be an issue as RhoA and Rac1 are closely related to each other, e.g., Rac1 can inhibit RhoA through PAK. Inhibition of both RhoA and Rac1 by DC-Rhoin may not achieve the best efficacy in downregulating RhoA activity for treating cancers. To the best of our knowledge, currently no small molecule RhoA inhibitors have demonstrated anticancer effects in small animal CRC experiments.

We sought to develop a RhoA subfamily-specific covalent inhibitor for CRC treatment by targeting the unique Cys16 on RhoA. To achieve this, we have established a chemoproteomics platform to screen out lead compounds targeting RhoA Cys16 *in vitro* through 2 rounds of gel-based ABPP experiments, first on RhoA and then on Rac1 and Cdc42. This approach roots on the unique residue Cys16 of RhoA among the three structurally similar Rho GTPases. Therefore, compounds that show positive results in the first screening with RhoA but negative results in the second screening with Rac1 and Cdc42 have a good opportunity to target RhoA Cys16 specifically. We anticipate that this screening strategy can be applied for the discovery of lead compounds targeting a specific Cys mutation in protein of interest. This high-throughput and cost-effective approach should be powerful in eliminating non-binders from a large compound library.

By the gel-based ABPP experiments, we have successfully identified lead covalent ligands with strong RhoA binding *in vitro*, with CL16 showing an IC_{50} of 440 nM for RhoA and no significant binding with Cdc42 and Rac1. Importantly, CL16 has demonstrated promising inhibitory effects on RhoA but not Rac1 and Cdc42 in CRC cells, as shown in the immunoblotting, immunofluorescence and/or FRET-RhoA biosensor experiments. This allows CL16 to exhibit anticancer and anti-metastatic effects in 2D and 3D CRC cell culture, as well as in 3 different mouse CRC xenograft models (HCT116, HT29, and metastatic SW620) and a mouse orthotropic CRC model. All these results highlight that CL16 should be a potential candidate for treating CRC through RhoA inhibition.

We have performed MS and chemoproteomics experiments to confirm Cys16 on RhoA as the primary binding site of CL16. In the literature, RhoA Cys16 has never been exploited as a binding site of covalent ligand, but it should be an ideal targetable site on RhoA to achieve high specificity over other small GTPases. This can be accounted for the uniqueness of Cys16 on RhoA according to sequence homology analysis, while Cys107, which is the binding site of the reported DC-Rhoin, is conserved in Rac1 and Cdc42. Functionally, Cys16 is located close to the nucleotide-binding pocket, as well as the switch I and switch II regions of RhoA. Structural analysis on CL16-RhoA binding by covalent docking reveals extensive interactions between CL16 and amino acid residues in the nucleotide-binding pocket. This, combined with the decrease in MANT-GTP (a fluorescent analog of GTP) binding onto RhoA protein and competitive binding with GDP in the gel-based ABPP experiments upon CL16 treatment, suggests that the irreversible binding onto RhoA Cys16 by CL16 could interfere with the GTP-RhoA binding to some extent, resulting in RhoA inhibition. In addition, decreases in RhoA-GEF and RhoA-GAP interactions have been observed in our co-immunoprecipitation experiments. A significant decrease in Dbs (a GEF protein)-induced MANT-GTP binding onto RhoA has also been found in the sample treated with CL16. These results indicate that CL16 binding onto RhoA Cys16 can disrupt interactions of RhoA with effector proteins. In view of the uniqueness on RhoA-subfamily and the functional bindings that can be achieved through covalent targeting, RhoA Cys16 should be a druggable hotspot for the development of therapeutic covalent ligands to inhibit RhoA-subfamily for cancer therapy.

Covalent docking also reveals a stronger RhoA binding from (*S*)-CL16 than from (*R*)-CL16 (Figures S7A and S7B), encouraging us to separate the racemate into two enantiomerically pure products, E1 and E2. E2 exhibited stronger effects in downregulating RhoA-GTP (Figure S7C) and slowing down CRC cell proliferation (Figure S7D) compared to the racemate, while E1 was found to be much less active and was the distomer. We are now working on the characterization of the stereochemistry of E1 and E2 by X-ray crystallography, with E2 likely being the (*S*)-CL16 as suggested by its biological activities. Future experiments will include investigating the efficacy of E2 in RhoA inhibition and antitumor effects *in vivo*, as well as using E1 as a negative control to confirm the mechanism of action of CL16.

Chemical biology experiments using CL16-alkyne as a molecular probe have been performed to validate target engagement of CL16 with RhoA by gel-based and MS-based ABPP experiments. It is noteworthy that RhoA is the only protein found in both MS-based target identification experiments on CL16-treated HCT116 cells and CL16-alkyne-probed HCT116 cells, and hence we are confident that RhoA is a protein target of CL16. Genetic mutation experiments show that inhibition of RhoA activity, cell proliferation, and cell migration are attributed to the covalent targeting of RhoA Cys16 in CRC cells. Notably, in the MS-based ABPP experiment, no significant binding of CL16 to other RhoA subfamily members (RhoB and RhoC) in CRC cells was found, despites their high sequence similarity with RhoA. CL16 also showed minimal inhibitory effects on RhoB and RhoC activity in CRC cells, suggesting that in the context of CRC, CL16 specifically targets RhoA Cys16 to mediate its biological activity. We have also demonstrated that CL16 exhibits promising antitumor effects on mouse CRC models with no observable toxicity, as evidenced by no significant changes in body weight and histology of major organ tissues. The minimal toxicity can be explained by the overexpression/hyperactivity of RhoA in CRC, as found in literature and confirmed in our

analysis of clinical data. This *in vivo* data highlight that covalent targeting of RhoA with good specificity should be an effective strategy for treating CRCs. Ongoing studies will investigate any on-target toxicity in other organs and tissues from CL16 treatment.

Notably, significant increases in $CD3^+$ T cells, including both $CD4^+$ and $CD8^+$ subsets have been found in the immunohistochemistry of tumor tissues from immunocompetent, orthotropic CRC mouse model treated with CL16. This indicates an increase in T cell infiltration into the tumor microenvironment. In literature, ROCK blockade has been reported to modulate functions of phagocytes, resulting in enhanced tumor cell phagocytosis and hence promoting T cell priming by dendritic cells.[64] The *in vivo* antitumor effects from CL16 should not originate from its effects on immune cells only because it significantly inhibits tumor growth in immunocompromised mice in the CRC xenograft experiments. Yet, this is possible for CL16 to inhibit RhoA signaling in immune cells, modulate their functions and trigger a stronger antitumor response in the immunocompetent mice. We are currently studying changes in functions and populations of immune cells after CL16 treatment, as well as acquiring a more comprehensive immune landscape by single-cell experiments to thoroughly decipher the anti-tumor effect of CL16. The effects of combination therapy of CL16 and immune checkpoint inhibitors on CRC will also be examined.

Limitations of the study

While we have examined the CL16-RhoA binding by computational covalent docking experiment, further investigations using X-ray crystallography or cryo-electron microscopy should provide better insights into the structural features of CL16-RhoA binding, as well as how the CL16 binding disrupts RhoA-GEF and RhoA-GAP interactions. In addition, CL16 may non-covalently bind to other proteins that cannot be detected by chemoproteomics experiments. Cellular thermal shift assay can be performed to investigate any of these non-covalent interactions involving CL16. Moreover, in this manuscript, we focused on studying the effects of CL16 on CRC cells. Since we observed changes in TME in immunocompetent mice after CL16 treatment, further comprehensive investigations are warranted to elucidate the effects of CL16 on immune cells and to evaluate the efficacy of combination therapy of CL16 and immune checkpoint inhibitors compared to monotherapy. Finally, large-scale animal experiments on studying toxicity, pharmacokinetics, and pharmacodynamics of CL16 will be critical for assessing its full potential for clinical applications.

RESOURCE AVAILABILITY

Lead contact

Further information and requests for resources and reagents should be directed to and will be fulfilled by the lead contact, Dr Clive Yik-Sham Chung (cyschung@hku.hk).

Materials availability

All unique/stable reagents generated in this study are available from the lead contact with a completed materials transfer agreement.

Data and code availability

- The mass spectrometry proteomics data have been deposited to the ProteomeXchange Consortium via the PRIDE partner repository and are publicly available as of the date of publication. Accession numbers are listed in the key resources table. The analyzed MS data are provided in Data S1 and S2. This paper also analyzes existing, publicly available RNA-seq data from TCGA cohort and GTEx database. These accession numbers for the datasets are listed in the key resources table. Source data including raw data and images, as well as data points for all our plots, is available in HKU Data Repository (https://doi.org/10.25442/hku.26807773). All data reported in this paper will be shared by the lead contact upon request.
- This paper does not report original code.
- Any additional information required to reanalyze the data reported in this paper is available from the lead contact upon request.

ACKNOWLEDGMENTS

C.Y.-S.C. acknowledges support from the Early Career Scheme (27315922) from University Grants Committee, Seed Fund for Basic Research for New Staff (202009185025) and Enhanced New Staff Start-up Research Grant from the University Research Committee and Li Ka Shing Faculty of Medicine, The University of Hong Kong (HKU). This work was also supported by the Center for Oncology and Immunology under the Health@InnoHK Initiative funded by the Innovation and Technology Commission, The Government of Hong Kong SAR, China. T.-Y.K. and J.Y.K.L. acknowledge the receipt of a University Postgraduate Fellowship and a Postgraduate Studentship administered by HKU respectively. H.Y.-Y.Y. acknowledges the receipt of a Hong Kong Postgraduate Fellowship Scheme and an HKU Presidential PhD Scholar Program administered by the University Grants Committee and The University of Hong Kong respectively. We thank Prof Martin Cheung at HKU for the FRET-RhoA biosensor construct and insightful inputs. We also thank Prof. Tatsuro Irimura at the University of Tokyo for sharing the mouse SL4 cells with us. We acknowledge the support from the Imaging and Flow Cytometry Core and Proteomics and Metabolomics Core, from the Center for PanorOmic Sciences (CPOS), Li Ka Shing Faculty of Medicine, HKU, on the confocal fluorescence microscopy imaging, flow cytometry, and MS experiments. We also thank Ms Bonnie Yan and Mr Ivan Lai, at the Departments of Chemistry and Microbiology, HKU, for their help in NMR experiments.

AUTHOR CONTRIBUTIONS

T.-Y.K., J.Y.K.L., and C.Y.-S.C. conceived the research. C.Y.-S.C., H.H.N.Y., and S.Y.L. obtained funding. T.-Y.K. performed *in vitro* characterization, covalent docking, co-immunoprecipitation, immunoblotting, chemical synthesis of CL16-alkyne, target identification, and study of the enantiomers. J.Y.K.L. performed screening experiments, chemical synthesis of CL16, co-immunoprecipitation, immunoblotting, and anticancer and antimetastatic studies. N.-S.L. performed GTP exchange assays, immunoblotting, and target validation using mutated cells. T.-Y.K. and J.C. performed experiments on the orthotopic mouse CRC models with supervision from J.Z. H.Y.-Y.Y. performed analysis on the clinical data and apoptosis assays. J.Y.K.L., I.B.H., and K.-Y.N. performed mouse xenografts experiments with supervision from S.M. H.H.N. Y. and S.Y.L. provided reagents and shared research expertise on cancer. C.Y.-S.C. performed fluorescence imaging, supervised the whole project and wrote the paper with input from all authors.

DECLARATION OF INTERESTS

A patent application from C.Y.-S.C., J.Y.K.L., T.-Y.K., and H.H.N.Y. has been filed for CL16 and CL16-alkyne, and the US patent application number is 63/579,246.

STAR★METHODS

Detailed methods are provided in the online version of this paper and include the following:

- KEY RESOURCES TABLE

SUPPLEMENTAL INFORMATION

Supplemental information can be found online at https://doi.org/10.1016/j.chembiol.2025.08.004.

Received: October 2, 2024
Revised: April 28, 2025
Accepted: August 14, 2025
Published: September 5, 2025

REFERENCES

1. Liu, H., Seynhaeve, A.L.B., Brouwer, R.W.W., van IJcken, W.F.J., Yang, L., Wang, Y., Chang, Z., and Ten Hagen, T.L.M. (2019). CREPT Promotes Melanoma Progression Through Accelerated Proliferation and Enhanced Migration by RhoA-Mediated Actin Filaments and Focal Adhesion Formation. Cancers (Basel) *12*, 33. https://doi.org/10.3390/cancers12010033.
2. Yang, N.Y., Pasquale, E.B., Owen, L.B., and Ethell, I.M. (2006). The EphB4 receptor-tyrosine kinase promotes the migration of melanoma cells through Rho-mediated actin cytoskeleton reorganization. J. Biol. Chem. *281*, 32574–32586. https://doi.org/10.1074/jbc.M604338200.
3. Cancer Genome Atlas Research Network (2014). Comprehensive molecular characterization of gastric adenocarcinoma. Nature *513*, 202–209. https://doi.org/10.1038/nature13480.
4. Kakiuchi, M., Nishizawa, T., Ueda, H., Gotoh, K., Tanaka, A., Hayashi, A., Yamamoto, S., Tatsuno, K., Katoh, H., Watanabe, Y., et al. (2014). Recurrent gain-of-function mutations of RHOA in diffuse-type gastric carcinoma. Nat. Genet. *46*, 583–587. https://doi.org/10.1038/ng.2984.
5. Yan, H.H.N., Siu, H.C., Law, S., Ho, S.L., Yue, S.S.K., Tsui, W.Y., Chan, D., Chan, A.S., Ma, S., Lam, K.O., et al. (2018). A Comprehensive Human Gastric Cancer Organoid Biobank Captures Tumor Subtype Heterogeneity and Enables Therapeutic Screening. Cell Stem Cell *23*, 882–897. https://doi.org/10.1016/j.stem.2018.09.016.
6. Wang, K., Yuen, S.T., Xu, J., Lee, S.P., Yan, H.H.N., Shi, S.T., Siu, H.C., Deng, S., Chu, K.M., Law, S., et al. (2014). Whole-genome sequencing and comprehensive molecular profiling identify new driver mutations in gastric cancer. Nat. Genet. *46*, 573–582. https://doi.org/10.1038/ng.2983.
7. Zhang, H., Schaefer, A., Wang, Y., Hodge, R.G., Blake, D.R., Diehl, J.N., Papageorge, A.G., Stachler, M.D., Liao, J., Zhou, J., et al. (2020). Gain-of-Function RHOA Mutations Promote Focal Adhesion Kinase Activation and Dependency in Diffuse Gastric Cancer. Cancer Discov. *10*, 288–305. https://doi.org/10.1158/2159-8290.CD-19-0811.
8. Zhang, S., Tang, Q., Xu, F., Xue, Y., Zhen, Z., Deng, Y., Liu, M., Chen, J., Liu, S., Qiu, M., et al. (2009). RhoA regulates G1-S progression of gastric cancer cells by modulation of multiple INK4 family tumor suppressors. Mol. Cancer Res. *7*, 570–580. https://doi.org/10.1158/1541-7786.MCR-08-0248.
9. Liu, S., Goldstein, R.H., Scepansky, E.M., and Rosenblatt, M. (2009). Inhibition of rho-associated kinase signaling prevents breast cancer metastasis to human bone. Cancer Res. *69*, 8742–8751. https://doi.org/10.1158/0008-5472.CAN-09-1541.
10. Wang, W., Goswami, S., Lapidus, K., Wells, A.L., Wyckoff, J.B., Sahai, E., Singer, R.H., Segall, J.E., and Condeelis, J.S. (2004). Identification and testing of a gene expression signature of invasive carcinoma cells within primary mammary tumors. Cancer Res. *64*, 8585–8594. https://doi.org/10.1158/0008-5472.CAN-04-1136.
11. Kalpana, G., Figy, C., Yeung, M., and Yeung, K.C. (2019). Reduced RhoA expression enhances breast cancer metastasis with a concomitant increase in CCR5 and CXCR4 chemokines signaling. Sci. Rep. *9*, 16351. https://doi.org/10.1038/s41598-019-52746-w.
12. Rodrigues, P., Macaya, I., Bazzocco, S., Mazzolini, R., Andretta, E., Dopeso, H., Mateo-Lozano, S., Bilić, J., Cartón-García, F., Nieto, R., et al. (2014). RHOA inactivation enhances Wnt signalling and promotes colorectal cancer. Nat. Commun. *5*, 5458. https://doi.org/10.1038/ncomms6458.
13. Jeong, D., Park, S., Kim, H., Kim, C.J., Ahn, T.S., Bae, S.B., Kim, H.J., Kim, T.H., Im, J., Lee, M.S., et al. (2016). RhoA is associated with invasion and poor prognosis in colorectal cancer. Int. J. Oncol. *48*, 714–722. https://doi.org/10.3892/ijo.2015.3281.
14. Messersmith, W.A. (2019). NCCN Guidelines Updates: Management of Metastatic Colorectal Cancer. J. Natl. Compr. Canc. Netw. *17*, 599–601. https://doi.org/10.6004/jnccn.2019.5014.
15. Siegel, R.L., Miller, K.D., and Jemal, A. (2019). Cancer statistics, 2019. CA Cancer J. Clin. *69*, 7–34. https://doi.org/10.3322/caac.21551.
16. Xie, Y.H., Chen, Y.X., and Fang, J.Y. (2020). Comprehensive review of targeted therapy for colorectal cancer. Signal Transduct. Target. Ther. *5*, 22. https://doi.org/10.1038/s41392-020-0116-z.
17. Schwartz, M. (2004). Rho signalling at a glance. J. Cell Sci. *117*, 5457–5458. https://doi.org/10.1242/jcs.01582.
18. Zandvakili, I., Lin, Y., Morris, J.C., and Zheng, Y. (2017). Rho GTPases: Anti- or pro-neoplastic targets? Oncogene *36*, 3213–3222. https://doi.org/10.1038/onc.2016.473.
19. O'Connor, K., and Chen, M. (2013). Dynamic functions of RhoA in tumor cell migration and invasion. Small GTPases *4*, 141–147. https://doi.org/10.4161/sgtp.25131.
20. Huang, B., Lu, M., Jolly, M.K., Tsarfaty, I., Onuchic, J., and Ben-Jacob, E. (2014). The three-way switch operation of Rac1/RhoA GTPase-based circuit controlling amoeboid-hybrid-mesenchymal transition. Sci. Rep. *4*, 6449. https://doi.org/10.1038/srep06449.
21. Eitaki, M., Yamamori, T., Meike, S., Yasui, H., and Inanami, O. (2012). Vincristine enhances amoeboid-like motility via GEF-H1/RhoA/ROCK/Myosin light chain signaling in MKN45 cells. BMC Cancer *12*, 469. https://doi.org/10.1186/1471-2407-12-469.
22. Cardama, G.A., Gonzalez, N., Maggio, J., Menna, P.L., and Gomez, D.E. (2017). Rho GTPases as therapeutic targets in cancer. Int. J. Oncol. *51*, 1025–1034. (Review). https://doi.org/10.3892/ijo.2017.4093.

23. Tatsuta, M., Iishi, H., Baba, M., Uedo, N., Ishihara, R., Higashino, K., Mukai, M., and Ishiguro, S. (2005). Induction by lysophosphatidic acid of peritoneal and pleural metastases of intestinal cancers induced by azoxymethane in Wistar rats. Cancer Lett. *219*, 137–145. https://doi.org/10.1016/j.canlet.2004.06.028.

24. Wang, H., Zhao, G., Liu, X., Sui, A., Yang, K., Yao, R., Wang, Z., and Shi, Q. (2010). Silencing of RhoA and RhoC expression by RNA interference suppresses human colorectal carcinoma growth in vivo. J. Exp. Clin. Cancer Res. *29*, 123. https://doi.org/10.1186/1756-9966-29-123.

25. Du, K., Wang, P., Liu, J., Ren, J., Zheng, G., Li, S., Chen, L., Hou, W., Hashida, H., Feng, F., and Zheng, J. (2024). Activation of RhoA/ROCK2 signaling by hypoxia-inducible factor 1alpha in promoting tumor growth and metastasis in human colon cancer. J. Gastrointest. Oncol. *15*, 237–249. https://doi.org/10.21037/jgo-23-844.

26. Ellenbroek, S.I.J., and Collard, J.G. (2007). Rho GTPases: functions and association with cancer. Clin. Exp. Metastasis *24*, 657–672. https://doi.org/10.1007/s10585-007-9119-1.

27. Shang, X., Marchioni, F., Sipes, N., Evelyn, C.R., Jerabek-Willemsen, M., Duhr, S., Seibel, W., Wortman, M., and Zheng, Y. (2012). Rational design of small molecule inhibitors targeting RhoA subfamily Rho GTPases. Chem. Biol. *19*, 699–710. https://doi.org/10.1016/j.chembiol.2012.05.009.

28. Sun, Z., Zhang, H., Zhang, Y., Liao, L., Zhou, W., Zhang, F., Lian, F., Huang, J., Xu, P., Zhang, R., et al. (2020). Covalent Inhibitors Allosterically Block the Activation of Rho Family Proteins and Suppress Cancer Cell Invasion. Adv. Sci. *7*, 2000098. https://doi.org/10.1002/advs.202000098.

29. Zhu, Y., Howard, G.A., Pittman, K., Boykin, C., Herring, L.E., Wilkerson, E. M., Verbanac, K., and Lu, Q. (2019). Therapeutic Effect of Y-27632 on Tumorigenesis and Cisplatin-Induced Peripheral Sensory Loss through RhoA-NF-kappaB. Mol. Cancer Res. *17*, 1910–1919. https://doi.org/10.1158/1541-7786.MCR-19-0024.

30. Barcelo, J., Samain, R., and Sanz-Moreno, V. (2023). Preclinical to clinical utility of ROCK inhibitors in cancer. Trends Cancer *9*, 250–263. https://doi.org/10.1016/j.trecan.2022.12.001.

31. Ozyigit, G., Onal, C., Igdem, S., Alicikus, Z.A., Iribas, A., Akin, M., Yalman, D., Cetin, I., Aksu, M.G., Atalar, B., et al. (2019). Treatment outcomes of prostate cancer patients with Gleason score 8-10 treated with definitive radiotherapy : TROD 09-001 multi-institutional study. Strahlenther. Onkol. *195*, 882–893. https://doi.org/10.1007/s00066-019-01476-z.

32. Wang, Q., Song, L.J., Ding, Z.B., Chai, Z., Yu, J.Z., Xiao, B.G., and Ma, C. G. (2022). Advantages of Rho-associated kinases and their inhibitor fasudil for the treatment of neurodegenerative diseases. Neural Regen. Res. *17*, 2623–2631. https://doi.org/10.4103/1673-5374.335827.

33. Limzerwala, J.F., Jeganathan, K.B., Kloeber, J.A., Davies, B.A., Zhang, C., Sturmlechner, I., Zhong, J., Fierro Velasco, R., Fields, A.P., Yuan, Y., et al. (2020). FoxM1 insufficiency hyperactivates Ect2-RhoA-mDia1 signaling to drive cancer. Nat. Cancer *1*, 1010–1024. https://doi.org/10.1038/s43018-020-00116-1.

34. Tsubaki, M., Genno, S., Takeda, T., Matsuda, T., Kimura, N., Yamashita, Y., Morii, Y., Shimomura, K., and Nishida, S. (2021). Rhosin Suppressed Tumor Cell Metastasis through Inhibition of Rho/YAP Pathway and Expression of RHAMM and CXCR4 in Melanoma and Breast Cancer Cells. Biomedicines *9*, 35. https://doi.org/10.3390/biomedicines9010035.

35. Zhou, W., Ercan, D., Chen, L., Yun, C.H., Li, D., Capelletti, M., Cortot, A.B., Chirieac, L., Iacob, R.E., Padera, R., et al. (2009). Novel mutant-selective EGFR kinase inhibitors against EGFR T790M. Nature *462*, 1070–1074. https://doi.org/10.1038/nature08622.

36. Ostrem, J.M., Peters, U., Sos, M.L., Wells, J.A., and Shokat, K.M. (2013). K-Ras(G12C) inhibitors allosterically control GTP affinity and effector interactions. Nature *503*, 548–551. https://doi.org/10.1038/nature12796.

37. Bradshaw, J.M., McFarland, J.M., Paavilainen, V.O., Bisconte, A., Tam, D., Phan, V.T., Romanov, S., Finkle, D., Shu, J., Patel, V., et al. (2015). Prolonged and tunable residence time using reversible covalent kinase inhibitors. Nat. Chem. Biol. *11*, 525–531. https://doi.org/10.1038/nchembio.1817.

38. Dubiella, C., Pinch, B.J., Koikawa, K., Zaidman, D., Poon, E., Manz, T.D., Nabet, B., He, S., Resnick, E., Rogel, A., et al. (2021). Sulfopin is a covalent inhibitor of Pin1 that blocks Myc-driven tumors in vivo. Nat. Chem. Biol. *17*, 954–963. https://doi.org/10.1038/s41589-021-00786-7.

39. Pinch, B.J., Doctor, Z.M., Nabet, B., Browne, C.M., Seo, H.S., Mohardt, M. L., Kozono, S., Lian, X., Manz, T.D., Chun, Y., et al. (2020). Identification of a potent and selective covalent Pin1 inhibitor. Nat. Chem. Biol. *16*, 979–987. https://doi.org/10.1038/s41589-020-0550-9.

40. Backus, K.M., Correia, B.E., Lum, K.M., Forli, S., Horning, B.D., González-Páez, G.E., Chatterjee, S., Lanning, B.R., Teijaro, J.R., Olson, A.J., et al. (2016). Proteome-wide covalent ligand discovery in native biological systems. Nature *534*, 570–574. https://doi.org/10.1038/nature18002.

41. Ramachandran, S., Makukhin, N., Haubrich, K., Nagala, M., Forrester, B., Lynch, D.M., Casement, R., Testa, A., Bruno, E., Gitto, R., and Ciulli, A. (2023). Structure-based design of a phosphotyrosine-masked covalent ligand targeting the E3 ligase SOCS2. Nat. Commun. *14*, 6345. https://doi.org/10.1038/s41467-023-41894-3.

42. Boike, L., Henning, N.J., and Nomura, D.K. (2022). Advances in covalent drug discovery. Nat. Rev. Drug Discov. *21*, 881–898. https://doi.org/10.1038/s41573-022-00542-z.

43. Cravatt, B.F. (2023). Activity-based protein profiling - finding general solutions to specific problems. Isr. J. Chem. *63*, e202300029. https://doi.org/10.1002/ijch.202300029.

44. Lentz, C.S., Sheldon, J.R., Crawford, L.A., Cooper, R., Garland, M., Amieva, M.R., Weerapana, E., Skaar, E.P., and Bogyo, M. (2018). Identification of a S. aureus virulence factor by activity-based protein profiling (ABPP). Nat. Chem. Biol. *14*, 609–617. https://doi.org/10.1038/s41589-018-0060-1.

45. Cravatt, B.F., Wright, A.T., and Kozarich, J.W. (2008). Activity-based protein profiling: from enzyme chemistry to proteomic chemistry. Annu. Rev. Biochem. *77*, 383–414. https://doi.org/10.1146/annurev.biochem.75.101304.124125.

46. Kuljanin, M., Mitchell, D.C., Schweppe, D.K., Gikandi, A.S., Nusinow, D.P., Bulloch, N.J., Vinogradova, E.V., Wilson, D.L., Kool, E.T., Mancias, J.D., et al. (2021). Reimagining high-throughput profiling of reactive cysteines for cell-based screening of large electrophile libraries. Nat. Biotechnol. *39*, 630–641. https://doi.org/10.1038/s41587-020-00778-3.

47. Boike, L., Cioffi, A.G., Majewski, F.C., Co, J., Henning, N.J., Jones, M.D., Liu, G., McKenna, J.M., Tallarico, J.A., Schirle, M., and Nomura, D.K. (2021). Discovery of a Functional Covalent Ligand Targeting an Intrinsically Disordered Cysteine within MYC. Cell Chem. Biol. *28*, 4–13. https://doi.org/10.1016/j.chembiol.2020.09.001.

48. Panyain, N., Godinat, A., Lanyon-Hogg, T., Lachiondo-Ortega, S., Will, E. J., Soudy, C., Mondal, M., Mason, K., Elkhalifa, S., Smith, L.M., et al. (2020). Discovery of a Potent and Selective Covalent Inhibitor and Activity-Based Probe for the Deubiquitylating Enzyme UCHL1, with Antifibrotic Activity. J. Am. Chem. Soc. *142*, 12020–12026. https://doi.org/10.1021/jacs.0c04527.

49. Conole, D., Cao, F., Am Ende, C.W., Xue, L., Kantesaria, S., Kang, D., Jin, J., Owen, D., Lohr, L., Schenone, M., et al. (2023). Discovery of a Potent Deubiquitinase (DUB) Small-Molecule Activity-Based Probe Enables Broad Spectrum DUB Activity Profiling in Living Cells. Angew. Chem. Int. Ed. Engl. *62*, e202311190. https://doi.org/10.1002/anie.202311190.

50. Bach, K., Beerkens, B.L.H., Zanon, P.R.A., and Hacker, S.M. (2020). Light-Activatable, 2,5-Disubstituted Tetrazoles for the Proteome-wide Profiling of Aspartates and Glutamates in Living Bacteria. ACS Cent. Sci. *6*, 546–554. https://doi.org/10.1021/acscentsci.9b01268.

51. Chiu, T.Y., Lazar, D.C., Wang, W.W., Wozniak, J.M., Jadhav, A.M., Li, W., Gazaniga, N., Theofilopoulos, A.N., Teijaro, J.R., and Parker, C.G. (2024). Chemoproteomic development of SLC15A4 inhibitors with anti-inflammatory activity. Nat. Chem. Biol. *20*, 1000–1011. https://doi.org/10.1038/s41589-023-01527-8.

52. Boatner, L.M., Palafox, M.F., Schweppe, D.K., and Backus, K.M. (2023). CysDB: a human cysteine database based on experimental quantitative

chemoproteomics. Cell Chem. Biol. *30*, 683–698. https://doi.org/10.1016/j.chembiol.2023.04.004.

53. Heindel, A.J., Brulet, J.W., Wang, X., Founds, M.W., Libby, A.H., Bai, D.L., Lemke, M.C., Leace, D.M., Harris, T.E., Hafner, M., and Hsu, K.L. (2023). Chemoproteomic capture of RNA binding activity in living cells. Nat. Commun. *14*, 6282. https://doi.org/10.1038/s41467-023-41844-z.
54. Shibolet, O., Giallourakis, C., Rosenberg, I., Mueller, T., Xavier, R.J., and Podolsky, D.K. (2007). AKAP13, a RhoA GTPase-specific guanine exchange factor, is a novel regulator of TLR2 signaling. J. Biol. Chem. *282*, 35308–35317. https://doi.org/10.1074/jbc.M704426200.
55. Tan, T.Z., Miow, Q.H., Miki, Y., Noda, T., Mori, S., Huang, R.Y.J., and Thiery, J.P. (2014). Epithelial-mesenchymal transition spectrum quantification and its efficacy in deciphering survival and drug responses of cancer patients. EMBO Mol. Med. *6*, 1279–1293. https://doi.org/10.15252/emmm.201404208.
56. Zhang, Y., Larraufie, M.H., Musavi, L., Akkiraju, H., Brown, L.M., and Stockwell, B.R. (2018). Design of Small Molecules That Compete with Nucleotide Binding to an Engineered Oncogenic KRAS Allele. Biochemistry *57*, 1380–1389. https://doi.org/10.1021/acs.biochem.7b01113.
57. Nobis, M., Herrmann, D., Warren, S.C., Strathdee, D., Cox, T.R., Anderson, K.I., and Timpson, P. (2020). Shedding new light on RhoA signalling as a drug target in vivo using a novel RhoA-FRET biosensor mouse. Small GTPases *11*, 240–247. https://doi.org/10.1080/21541248.2018.1438024.
58. Pertz, O., Hodgson, L., Klemke, R.L., and Hahn, K.M. (2006). Spatiotemporal dynamics of RhoA activity in migrating cells. Nature *440*, 1069–1072. https://doi.org/10.1038/nature04665.
59. Pradhan, R., Ngo, P.A., Martinez-Sanchez, L.D., Neurath, M.F., and Lopez-Posadas, R. (2021). Rho GTPases as Key Molecular Players within Intestinal Mucosa and GI Diseases. Cells *10*, 66. https://doi.org/10.3390/cells10010066.
60. Zhang, G.Y., Yang, W.H., and Chen, Z. (2016). Upregulated STAT3 and RhoA signaling in colorectal cancer (CRC) regulate the invasion and migration of CRC cells. Eur. Rev. Med. Pharmacol. Sci. *20*, 2028–2037.
61. Canon, J., Rex, K., Saiki, A.Y., Mohr, C., Cooke, K., Bagal, D., Gaida, K., Holt, T., Knutson, C.G., Koppada, N., et al. (2019). The clinical KRAS (G12C) inhibitor AMG 510 drives anti-tumour immunity. Nature *575*, 217–223. https://doi.org/10.1038/s41586-019-1694-1.
62. Morimoto-Tomita, M., Ohashi, Y., Matsubara, A., Tsuiji, M., and Irimura, T. (2005). Mouse colon carcinoma cells established for high incidence of experimental hepatic metastasis exhibit accelerated and anchorage-independent growth. Clin. Exp. Metastasis *22*, 513–521. https://doi.org/10.1007/s10585-005-3585-0.
63. Dopeso, H., Rodrigues, P., Bilic, J., Bazzocco, S., Cartón-García, F., Macaya, I., de Marcondes, P.G., Anguita, E., Masanas, M., Jiménez-Flores, L.M., et al. (2018). Mechanisms of inactivation of the tumour suppressor gene RHOA in colorectal cancer. Br. J. Cancer *118*, 106–116. https://doi.org/10.1038/bjc.2017.420.
64. Nam, G.H., Lee, E.J., Kim, Y.K., Hong, Y., Choi, Y., Ryu, M.J., Woo, J., Cho, Y., Ahn, D.J., Yang, Y., et al. (2018). Combined Rho-kinase inhibition and immunogenic cell death triggers and propagates immunity against cancer. Nat. Commun. *9*, 2165. https://doi.org/10.1038/s41467-018-04607-9.
65. Liu, J.A., Rao, Y., Cheung, M.P.L., Hui, M.N., Wu, M.H., Chan, L.K., Ng, I. O.L., Niu, B., Cheah, K.S.E., Sharma, R., et al. (2017). Asymmetric localization of DLC1 defines avian trunk neural crest polarity for directional delamination and migration. Nat. Commun. *8*, 1185. https://doi.org/10.1038/s41467-017-01107-0.
66. Ozdamar, B., Bose, R., Barrios-Rodiles, M., Wang, H.R., Zhang, Y., and Wrana, J.L. (2005). Regulation of the polarity protein Par6 by TGFbeta receptors controls epithelial cell plasticity. Science *307*, 1603–1609. https://doi.org/10.1126/science.1105718.
67. Wang, X.L., Wan, K., and Zhou, C.H. (2010). Synthesis of novel sulfanilamide-derived 1,2,3-triazoles and their evaluation for antibacterial and antifungal activities. Eur. J. Med. Chem. *45*, 4631–4639. https://doi.org/10.1016/j.ejmech.2010.07.031.
68. Goksen, U.S., Sarigul, S., Bultinck, P., Herrebout, W., Dogan, I., Yelekci, K., Ucar, G., and Gokhan Kelekci, N. (2019). Absolute configuration and biological profile of pyrazoline enantiomers as MAO inhibitory activity. Chirality *31*, 21–33. https://doi.org/10.1002/chir.23027.
69. Subramanian, A., Tamayo, P., Mootha, V.K., Mukherjee, S., Ebert, B.L., Gillette, M.A., Paulovich, A., Pomeroy, S.L., Golub, T.R., Lander, E.S., and Mesirov, J.P. (2005). Gene set enrichment analysis: a knowledge-based approach for interpreting genome-wide expression profiles. Proc. Natl. Acad. Sci. USA *102*, 15545–15550. https://doi.org/10.1073/pnas.0506580102.
70. Mootha, V.K., Lindgren, C.M., Eriksson, K.F., Subramanian, A., Sihag, S., Lehar, J., Puigserver, P., Carlsson, E., Ridderstråle, M., Laurila, E., et al. (2003). PGC-1alpha-responsive genes involved in oxidative phosphorylation are coordinately downregulated in human diabetes. Nat. Genet. *34*, 267–273. https://doi.org/10.1038/ng1180.
71. Mons, E., Roet, S., Kim, R.Q., and Mulder, M.P.C. (2022). A Comprehensive Guide for Assessing Covalent Inhibition in Enzymatic Assays Illustrated with Kinetic Simulations. Curr. Protoc. *2*, e419. https://doi.org/10.1002/cpz1.419.

STAR★METHODS

KEY RESOURCES TABLE

REAGENT or RESOURCE	SOURCE	IDENTIFIER
Antibodies		
Anti-RhoA	Cell Signaling Technology	Cat# 2117S; RRID:AB_10693922
Anti-MLC2	Cell Signaling Technology	Cat# 3672S; RID:AB_10692513
Anti-phospho-MLC2 (Ser19)	Cell Signaling Technology	Cat# 3671S; RRID:AB_330248
Anti-Rac1/2/3	Cell Signaling Technology	Cat# 2465S; RRID:AB_2176152
Anti-cdc42	Cell Signaling Technology	Cat# 2462S; RRID:AB_2078085
Anti-p21	Cell Signaling Technology	Cat# 2947S; RRID:AB_823586
Anti-p27	Cell Signaling Technology	Cat# 3686S; RRID:AB_2077850
Anti-cyclin A2	Cell Signaling Technology	Cat# 4656S; RRID:AB_2071958
Anti-cyclin B1	Cell Signaling Technology	Cat# 4138S; RRID:AB_2072132
Anti-GAPDH	Cell Signaling Technology	Cat# 5174S; RRID:AB_10622025
Anti-beta-Actin	Cell Signaling Technology	Cat# 3700S; RRID:AB_2242334
Anti-GFP	Cell Signaling Technology	Cat# 2956S; RRID:AB_1196615
Anti-DYKDDDDK tag	Cell Signaling Technology	Cat# 8146S; RRID:AB_10950495
Anti-GST tag	Cell Signaling Technology	Cat# 2624S; RRID:AB_2189875
Anti-CD3	Cell Signaling Technology	Cat# 78588S; RRID:AB_2889902
Anti-CD4	Cell Signaling Technology	Cat# 25229S; RRID:AB_2798898
Anti-CD8	Cell Signaling Technology	Cat# 98941S; RRID:AB_2756376
Anti-Ki67	Cell Signaling Technology	Cat# 12202; RRID:AB_2620142
Anti-cleaved caspase 3 (Asp175)	Cell Signaling Technology	Cat# 9661S; RRID:AB_2341188
Anti-VEGFR2	Cell Signaling Technology	Cat# 2479S; RRID:AB_2212507
Anti-VEGFA	Abcam	Cat# 1316; RRID:AB_299738
Anti-α-tubulin	Cell Signaling Technology	Cat# 2144; RRID:AB_2210548
Bacterial and virus strains		
BL21(DE3) Competent Cells	Thermo Fisher Scientific	Cat# EC0114
DH5α Competent Cells	Thermo Fisher Scientific	Cat# EC0112
Chemicals, peptides, and recombinant proteins		
RhoA	Abcam	Cat# 101594
His-RhoA	Cytoskeleton	Cat# RH01-A
His-Dbs DH/PH	Cytoskeleton	Cat# GE01-A
MANT-GTP	Thermo Fisher Scientific	Cat# M12415
Rhosin	Sigma-Aldrich	Cat# 555460
Azide-fluor 545	Sigma-Aldrich	Cat# 760757
Iodoacetamide	Sigma-Aldrich	Cat# I6125
Copper(II) sulfate pentahydrate	Sigma-Aldrich	Cat# 678937
Tris(2-carboxyethyl)phosphine hydrochloride (TCEP)	Sigma-Aldrich	Cat# C4706
Tris[(1-benzyl-1H-1,2,3-triazol-4-yl)methyl] amine (TBTA)	Cayman Chemical	Cat# 18816
Desthiobin-PEG3-Azide	Sigma-Aldrich	Cat# 902020
Iodoacetamide-rhodamine (IA-Rh)	Setareh Biotech	Cat# 6222
B-PER™ Bacterial Protein Extraction Reagent	Thermo Fisher Scientific	Cat# 78243
Propidium Iodide	Thermo Fisher Scientific	Cat# P3566
CellEvent™ Caspase-3/7 Detection Reagents	Thermo Fisher Scientific	Cat#C10423

(*Continued on next page*)

CellPress
OPEN ACCESS

Continued

REAGENT or RESOURCE	SOURCE	IDENTIFIER
Alexa Fluor® 488 Phalloidin	Cell Signaling Technology	Cat# 8878S
3-(4,5-Dimethylthiazol-2-yl)-2,5-diphenyltetrazolium bromide (MTT)	Macklin	Cat# T6126
Critical commercial assays		
RhoA Activation Assay Biochem Kit	Cytoskeleton	Cat# BK036
Rac1 Pull-Down Activation Assay Biochem Kit	Cytoskeleton	Cat# BK035
Deposited data		
RNA-Seq result from TCGA cohort (TCGA-COAD and TCGA-READ)	NIH	https://portal.gdc.cancer.gov/
RNA-Seq result from GTEx portal	NIH	https://www.gtexportal.org/home/
Proteomic data	This paper	PRIDE ID: PXD053036 and PXD053041
Experimental models: Cell lines		
Human: HEK293T	ATCC	#CRL-3216
Human: HCT116	ATCC	#CCL-247
Human: HT29	ATCC	#HTB-38
Human: SW620	ATCC	#CCL-227
Human: SW480	ATCC	#CCL-228
Human: LOVO	ATCC	#CCL-229
Human: CCD-18Co	ATCC	#CRL-1459
Mice: SL4	Morimoto-Tomita et al.[62]	N/A
Experimental models: Organisms/strains		
Mouse: BALB/c nude mice	Centre for Comparative Medicine Research, HKU	RRID: MGI:2161072
Mouse: C57BL/6 immunocompetent mice	Laboratory Animal Services Centre, CUHK	RRID: MGI:2159769
Oligonucleotides		
ON-TARGETplus Human RHOA siRNA	Horizon	Cat# LQ-003860-00-0010
ON-TARGETplus Human RHOB siRNA SMARTpool	Horizon	Cat# L-008395-00-0005
ON-TARGETplus Human RHOC siRNA SMARTpool	Horizon	Cat# L-008555-00-0005
FRET RhoA biosensor	Prof Martin Cheung's Laboratory[65]	N/A
Flag-RhoA	Ozdama et al.[66]	Addgene # 11750
pGEX-2T-Cdc42-wt	A gift from Gary Bokoch	Addgene # 12969
pGEX-2T-Rac1-wt	A gift from Gary Bokoch	Addgene # 12977
pGEX-2T-RhoA-wt	A gift from Gary Bokoch	Addgene # 12959
pGEX-2T-RhoA-T19N	A gift from Gary Bokoch	Addgene # 12960
Software and algorithms		
R 4.3.0	N/A	https://cran.r-project.org/
GSEA v4.3.3	MsigDB	https://www.gsea-msigdb.org/gsea/index.jsp
ImageJ	National Institutes of Health	https://imagej.net/ij/
GraphPad Prism 9	GraphPad Software	https://www.graphpad.com/
MaxQuant v2.0.3.0	Max-Planck-Institute of Biochemistry	https://www.maxquant.org/
MSFragger v3.7	Nesvizhskii lab	https://msfragger.nesvilab.org/
Maestro 13.4	Schrödinger	https://www.schrodinger.com/platform/products/maestro/
Other		
Sequencing grade modified trypsin	Promega	Cat# V51111

EXPERIMENTAL MODEL AND STUDY PARTICIPANT DETAILS

Cell culture

All cell lines except SL4 were purchased from ATCC without further authenticated. SL4 cells (sex of cell: female)[62] were obtained from Prof. Tatsuro Irimura at the University of Tokyo and were not further authenticated. Cell lines were cultured in 37°C incubator with 5% CO_2. HT29 (ATCC, HTB-38, sex of cell: female) and HEK293T (ATCC, CRL-3216, sex of cell: female) were cultured in DMEM. Of note, engineered HT29 was cultured in Mccoy's 5A. SW620 (ATCC, CCL-227, sex of cell: male), SW480 (ATCC, CCL-228, sex of cell: male), LOVO (ATCC, CCL-229, sex of cell: male) and HCT116 (ATCC, CCL-247, sex of cell: male) were cultured in RPMI. CCD-18Co (ATCC, CRL-1459, sex of cell: female) was cultured in MEM. SL4 was cultured in DMEM/F12. Unless specified, all media were purchased from Gibco and supplemented with 10% FBS and 1% penicillin and streptomycin prior use.

Generation of HT29 expressing *RhoA*^{C16A}

HT29 cells with RhoA C16A knock-in were prepared by BrainVTA using the CRISPR-Cas9 technique on ATCC provided cells. Briefly, HT29 cells were transfected with RhoA construct with mutated loci in CRISPR/Cas9 vector (U6-sa-sgRNA) using PEI. Cells were subsequently selected with 2 μg/mL puromycin and 800 μg/mL neomycin for 2 weeks. Monoclonal cells were then selected, propagated and subjected to Sanger sequencing to validate the homozygous C16A amino acid substitution (GCT to TGT) in RhoA gene.

Animals

All mouse experiments were approved by and performed in accordance with the Committee of the Use of Live Animals in Teaching and Research (CULATR) at The University of Hong Kong or Animal Experimentation Ethics Committee of The Chinese University of Hong Kong (CUHK-AEEC). Experiments also obeyed the Animals (Control of Experiments) Ordinance of Hong Kong. 7-week-old male BALB/c mice with weight around 20 g used in this study. They were housed in pathogen-free and controlled conditions in individually ventilated cages and fed an irradiated soy-free diet and autoclaved tap water *ad libitum*. CRC cell suspensions (HCT116 $2x10^6$ cells per mouse, HT29 $3x10^6$ cells per mouse or SW620 $1x10^6$ cells per mouse) resuspended in Matrigel/PBS were inoculated into mice subcutaneously at the lower right dorsal side of BALB/c nude mice. CL16 was dissolved in PET (60% PEG400, 30% Ethanol, 10% Tween80, v/v) with sonication until the solution was clear, followed by 1:1 dilution in PBS to prepare the solution for injection. CL16 was injected intraperitoneally (200 μL) every 2 days when tumor has reached 100 mm^3 in size, until humane endpoint was reached. The tumor volume and body weight of the mice were measured throughout the treatment. The tumor volume was calculated by the equation.

$$Volum\left(mm^3\right) = 1 \times w^2 / 2$$

where l and w were the length and width of the tumor at the end of the treatment, the mice were sacrificed and the tumor weight was measured. The tissues from the tumor and other major organs were then processed into formalin-fixed, paraffin-embedded (FFPE) blocks, and proceeded to immunohistochemistry analysis.

In the orthotropic model, seven- to eight-week-old C57BL/6 mice with weight around 20 g were anesthetized by ketamine–xylazine to incorporated 1×10^6 SL4 cells in PBS intracecally. One week post-surgery, CL16 or solvent control was injected intraperitoneally (200 μL) for two weeks as described above. Subsequent procedure and tissue processing were performed following aforementioned methods.

METHOD DETAILS

Chemical synthesis and characterization

CL1−CL199 were purchased from Enamine LLC with purity of >95%. They were used in the screening experiments. After identification of CL16 as the lead compound, it was re-synthesized and the purity was >98% as found in the UPLC characterization. All the characterization data of CL16 and CL16-alkyne can be found in Data S3. 2-Acetyl-benzofuran, chloroacetyl chloride and propargyl bromide were purchased from Macklin. Hydrazine monohydrate, 2-acetyl-7-hydroxybenzofuran and potassium carbonate were purchased from TCI. Furfural, triethylamine and sodium hydroxide were purchased from Dieckmann whereas sodium hydroxide was purchased from Aladin. All other reagents were of analytical grade and were used without further purification. MilliQ water was used in all experiments unless otherwise stated.

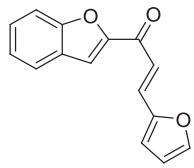

1a

1a was synthesized according to the reported literature.[67]

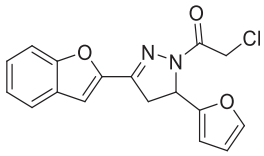

CL16

Hydrazine (2 equiv.) was added to **1a** (1 equiv.) in ethanol and heat under reflux for 3-4 hours. Any organic volatile was evaporated under reduced pressure, then the residue was extracted with dichloromethane. The dichloromethane layer was dried over $MgSO_4$, filtered and evaporated to dryness. Then the intermediate was dissolved in dry dichloromethane, chloroacetyl chloride (1.2 equiv.) and triethylamine (2 equiv.) were added dropwise slowly on ice. The reaction was allowed to proceed overnight. Any volatile organic solvent was evaporated under reduced pressure, and the crude product was purified by column chromatography on silica gel using hexane/ethyl acetate (80:20, v/v) as eluent to afford **CL16**. ^{1}H NMR (600 MHz, Chloroform-d) δ 7.66 – 7.54 (m, 2H), 7.44 – 7.39 (m, 1H), 7.34 – 7.27 (m, 2H), 7.16 (s, 1H), 6.45 – 6.29 (m, 2H), 5.73 (dd, J = 11.7, 4.8 Hz, 1H), 4.65 – 4.53 (m, 2H), 3.70 – 3.53 (m, 2H). ^{13}C NMR (151 MHz, Chloroform-d) δ 164.14, 155.63, 150.46, 147.68, 147.18, 142.37, 127.68, 126.71, 123.74, 121.87, 111.80, 110.73, 109.72, 108.73, 53.82, 42.35, 37.72. HRMS (ESI+): m/z calc for $C_{17}H_{14}ClN_2O_3$ [M+H]+ 329.0693; observed 329.0698.

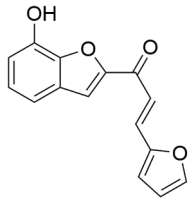

1b

1b was synthesized according to the same procedure as **1a** except using 2-acetyl-7-hydroxybenzofuran instead of 2-acetylbenzofuran. The crude product was purified by column chromatography on silica gel using hexane/ ethyl acetate (60:40, v/v) as eluent, yielding **1b** as a yellow solid. ^{1}H NMR (600 MHz, Chloroform-*d*) δ 7.70 (d, *J* = 15.3 Hz, 1H), 7.65 (s, 1H), 7.57 (d, *J* = 1.8 Hz, 1H), 7.43 (d, *J* = 15.3 Hz, 1H), 7.28 (dd, *J* = 7.9, 1.0 Hz, 2H), 7.21 (t, *J* = 7.8 Hz, 1H), 7.03 (ddd, *J* = 7.0, 5.9, 1.1 Hz, 1H), 6.79 (d, *J* = 3.4 Hz, 1H), 6.55 (dd, *J* = 3.4, 1.8 Hz, 1H). ESI-MS (m/z): $[M+H]^+$ 255.1.

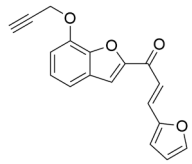

2b (1.0 equiv.) was dissolved in acetonitrile. Propargyl bromide (1.5 equiv.) and K_2CO_3 (2.5 equiv.) was added to the solution mixture and heated under reflux overnight. The reaction mixture was quenched by adding water and dried under reduced pressure, then the aqueous layer was extracted with dichloromethane. The organic layer was dried by $MgSO_4$, filtered and evaporated under reduced pressure. The crude product was purified by column chromatography on silica gel using hexane/ethyl acetate (80:20, v/v) as eluent to afford the compound **2b**. ^{1}H NMR (600 MHz, Chloroform-*d*) δ 7.70 (d, *J* = 15.4 Hz, 1H), 7.62 (s, 1H), 7.57 (s, 1H), 7.52 (d, *J* = 15.4 Hz, 1H), 7.35 (d, *J* = 7.4 Hz, 1H), 7.22-7.27 (m, 1H), 7.11 (d, *J* = 7.9 Hz, 1H), 6.78 (d, *J* = 3.4 Hz, 1H), 6.53-6.54 (m, 1H), 4.97 (d, *J* = 2.4 Hz, 2H), 2.58 (t, *J* = 2.4 Hz, 1H). ESI-MS (m/z): $[M+H]^+$ 293.3.

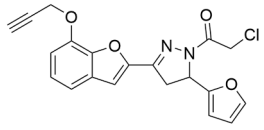

Hydrazine (2 equiv.) was added to **2b** (1 equiv.) in ethanol and heat under reflux for 3-4 hours. Any organic volatile was evaporated under reduced pressure, then the residue was extracted with dichloromethane. The dichloromethane layer was dried over $MgSO_4$, filtered and evaporated to dryness. Then the intermediate was dissolved in dry dichloromethane, chloroacetyl chloride (1.2 equiv.) and triethylamine (2 equiv.) were added dropwise slowly on ice. The reaction was allowed to proceed overnight. Any volatile organic solvent was evaporated under reduced pressure, and the crude product can be purified by column chromatography on silica gel using hexane/ethyl acetate (80:20, v/v) as eluent to afford **CL16-alkyne**. ^{1}H NMR (600 MHz, Chloroform-*d*) δ 7.30 (d, *J* = 1.8 Hz, 1H),

7.27 (d, *J* = 7.4 Hz, 1H), 7.21 (d, *J* = 7.9 Hz, 1H), 7.16 (d, *J* = 3.6 Hz, 1H), 7.04 (dd, *J* = 7.9, 1.1 Hz, 1H), 6.40 (d, *J* = 3.3 Hz, 1H), 6.32 (dd, *J* = 3.3, 1.8 Hz, 1H), 5.71 (dd, *J* = 11.6, 4.9 Hz, 1H), 4.93 (d, *J* = 2.4 Hz, 2H), 4.59 (q, *J* = 14.3 Hz, 2H), 3.66 (dd, *J* = 17.6, 11.7 Hz, 1H), 3.57 (dd, *J* = 17.6, 4.9 Hz, 1H), 2.57 (t, *J* = 2.4 Hz, 1H). ^{13}C NMR (151 MHz, Chloroform-*d*) δ 171.21, 164.20, 164.18, 150.47, 148.04, 147.88, 147.26, 147.16, 145.18, 144.46, 143.23, 142.34, 132.89, 130.03, 129.72, 129.55, 124.36, 124.29, 118.35, 116.32, 114.98, 114.83, 114.13, 110.69, 110.42, 109.98, 109.54, 109.48, 109.40, 108.65, 108.62, 78.06, 76.31, 76.22, 69.94, 60.41, 56.76, 53.83, 42.35, 42.30, 37.85, 37.82, 29.69, 21.05, 14.19. HRMS (ESI+): m/z calc for $C_{20}H_{16}ClN_2O_4$ [M+H]+ 383.0799; observed 383.0796.

Separation of CL16 racemate into enantiomerically pure products, E1 and E2

CL16 racemate (47 mg) was separated by liquid chromatography using EnantioPak®Y1 column to afford E1 (16.1 mg) and E2 (18.5 mg), which were eluted at 7.72 and 10.67 min respectively.

Based on our covalent docking results (Figures S3A and S3B), the (*S*)-enantiomer of CL16 gives a more negative docking score compared to the (*R*)-enantiomer, suggesting a more favorable binding to RhoA. We found that E2 exhibited more promising RhoA inhibitory effects and anticancer properties compared to the racemate (Figures S7C and S7D), while E1 showed much lower activities. In addition, from a previous study on the separation of pyrazoline enantiomers by chiral column and subsequent characterization of the stereochemistry by vibrational circular dichroism[68] the enantiomer first eluted from the chiral column (CHIRALPAK AD-H; a different chiral column from our experiment) was the (*R*)-enantiomer. This further suggests that E1 and E2 are likely the (*R*)- and (*S*)-CL16 respectively.

Gene set enrichment analysis (GSEA)

Unstranded TPM values from open-access colorectal adenocarcinoma tumour tissue RNA-seq results obtained from TCGA were used for analysis and GSEA v4.3.3 was used for computation.[69,70] In comparing stages 0-I and IV, the results were divided according to AJCC pathological stages. To compare high and low EMT scores[55] the EMT scores were computed for all samples using single sample gene set enrichment scores (ssGSEAs) through the hacksig R package. The scores were separated into two groups, relative to the median score.

Gel-based activity-based protein profiling (ABPP) for screening

Recombinant human RhoA (0.1 μg; ab101594) was pretreated with cysteine-reactive compounds (20 μM) or DMSO for 1 hour at room temperature, followed by incubation with iodoacetamide-rhodamine (IA-Rh; 1 μM) for 1 hour at room temperature. The reaction was then quenched by boiling in sampling buffer and samples were subjected to SDS-PAGE to separate proteins bands. In-gel fluorescence intensity was measured with a Chemidoc using setting for Rhodamine. Gel was subsequently stained with silver stain (Pierce) for visualization of protein content and covalent modification. Band intensity was quantified using ImageJ. Covalent ligands, that showed lower than 30% of the ratio (in-gel fluorescence/silver stain) and retained at least 70% intensity in the silver stain compared to the DMSO control, were considered as lead compounds.

Covalent docking

Schrödinger Maestro 13.4 was used for covalent docking. Structure of GDP-bound RhoA (PDB:1CC0) and CL16 ligand were prepared using the protein preparation wizard and LigPrep module respectively by default setting. Covalent docking was performed by CovDoc algorithm with nucleophilic substitution selected as reaction type.

Fluorescence assays on RhoA-GTP binding

For GTP binding onto RhoA in the absence of RhoGEF, 2 μL of purified recombinant human RhoA protein (0.75 μg; Cytoskeleton #RH01) was dissolved in 11 μL of GTP-exchange buffer (20 mM Tris, 50 mM NaCl, 10 mM $MgCl_2$, pH 7.5) in a 384-well plate. 1 μL of DMSO, CL16 or Rhosin was added to the solution, and the mixture was incubated at room temperature for 1 h. After that, 2 μL of GTP-MANT (5.6 μM; ThermoFisher Scientific #M12415) was added to the solution and the fluorescence was measured at 448±30 nm with photoexcitation at 356±30 nm using a plate reader (Clariostar) at every 30 s for 3 h.

For Dbs-mediated GTP binding onto RhoA, 2 μL of purified recombinant human RhoA protein was dissolved in 8 μL of GTP-exchange buffer in a 384-well plate. 1 μL of DMSO, CL16 or Rhosin was added to the solution, and the mixture was incubated at room temperature for 1 h. After that, 2 μL of GTP-MANT was added to the solution and the fluorescence was measured at 448 ±30 nm with photoexcitation at 356±30 nm using a plate reader (Clariostar) at every 30 s for 5 cycles. Then, 3 μL of recombinant human Dbs protein (0.3 μg; Cytoskeleton #GE01) was added to the solution mixture and the fluorescence measurement was resumed for every 30 s at room temperature.

MTT assay

HCT116 (2,500 cells/well), HT29 (4,000 cells/well), LOVO (4,000 cells/well), SW620 (4,000 cells/well), CCD-18Co (10,000 cells/well) or SW480 (12,000 cells/well) were plated in 96-well plate in triplicates. Cells were treated with concentration gradient of CL16 for 48 hours. Then, the cells were incubated with MTT solution (5 mg/mL) at 37°C with 5% CO_2 for 4 hours. Cells were then lyzed in 10% SDS in 0.01M HCl, and their absorption at 570 nm were measured by Perkin Elmer Victor 3 (Molecular Devices). IC_{50} values were analyzed by nonlinear best-fit regression using Prism Graphpad 9.

CellPress
OPEN ACCESS

Wound healing assay

HT29 cells were plated in a 24-well plate at *ca.* 90% confluency. On the next day, a wound was scratched using a P-20 tip. Followed by the removal of cell debris in PBS, CL16 or Rhosin in complete medium was added to the cells. Wound closure was recorded every 24 hours under light microscope with 10× objective and wound area was measured by ImageJ.

Matrigel invasion assay

SW620 cells (1 x 10^5 cells per well) in serum-free medium with solvent vehicle, CL16 or Rhosin were plated in a Boyden chamber. Complete RPMI medium was loaded into the lower chamber as chemoattractant. After 24 h, the bottom of Boyden chamber was fixed by 4% paraformaldehyde for 10 min and then stained with crystal violet solution for another 10 min. Excess stain was washed out by tap water. Invaded cells were recorded under light microscope with 10× objective and quantified by ImageJ.

Proliferation assay

HT29 cells (5 × 10^4 cells per well) were plated in a 24-well plate in complete medium with CL16 at indicated concentrations. After 48 h, the cells were rinsed with PBS, fixed by 4% paraformaldehyde for 10 min and then stained with crystal violet solution for another 10 min. Excess stain was washed out by tap water. Viable cells were imaged under light microscope with 10× objective and quantified by ImageJ.

Spheroid formation assay

HT29 and SW620 (5,000 cells) were inoculated in serum-free DMEM/F12 medium with 20 ng/mL epithelial growth factor (EGF) in 96-well round-bottom low-affinity plate (Nunc). Medium was supplemented with CL16 or Rhosin when spheroid has formed an opaque core. Images were recorded under a light microscope with 10× objective.

FRET RhoA biosensor to image cellular RhoA activity

HCT116 and HT29 cells were plated on a 8-well Nunc Lab-Tek chambered slide system and allowed to grow in complete medium at 37°C with 5% CO_2 to *ca.* 30 and 50% confluency respectively. The cells were then transfected with the FRET RhoA biosensor construct (a gift from Prof Martin Cheung at the University of Hong Kong) and Lipofectamine 2000 (ThermoFisher Scientific) for 48 h according to manufacturer's instruction. The transfected cells were starved in serum-free DMEM with CL16 (10 μM) or solvent vehicle for 24 h, followed by re-stimulation with 10% FBS for 10 min. The cells were then washed with PBS and imaged in Hanks' Balanced Salt Solution (HBSS) by confocal fluorescence microscopy. The cells were excited at a 458 nm diode laser, and mTFP1 emission was collected on a META detector between 470 and 495 nm, while FRET channel was collected on a META detector between 516 and 550 nm. Image analysis was performed by use of ImageJ, with FRET/mTFP1 images generated by the Ratio Plus plugin of ImageJ. For quantification, a region of interest (ROI) was created around individual cell, and cellular FRET/mTFP1 was measured. The reported FRET/mTFP1 was determined by averaging the measured intensity from 10 different cells from 3 different biological replicates/group.

siRNA knockdown

HT29 cells (3x10^6 cells) in 6-well plate were transfected with si*RHOA, siRHOB or siRHOC* (5 μM; Horizon #L-003560-00-0010, L-008395-00-0005 or L-008555-00-0005) using Dharmafect1 reagent (Horizon) for 48 hours. The target gene expression was then examined by immunoblotting.

Immunoblotting and immunohistochemistry (IHC)

For Western blot analysis, cells were washed with PBS and then harvested using cell lysis buffer (1% Triton X100, 10 mM beta glycerol phosphate, 10 mM sodium pyrophosphate, 40 mM HEPES, 4 mM EDTA, pH7.4) with 4% protease/phosphatase inhibitor cocktail (Pierce). Cell debris were removed by centrifugation at 5,000*g* for 10 min at 4°C. The protein concentration of the lysates was quantified by BCA assay (Pierce), normalized, denatured by boiling in sampling buffer, and separated in 10% polyacrylamide gel (Biorad). Subsequent detection of proteins is identical to established Western blot procedure. All primary antibodies were diluted 1:1000 in 5% BSA/milk in TBST with 1% NaN_3.

For tumor samples, proteins were extracted by homogenization of the tumor tissues (~10 mm^3) in RIPA lysis buffer supplemented with 4% protease/phosphatase inhibitor cocktail (Pierce). The homogenates were snap-frozen and thawed for better protein extraction. Clarified proteins samples were normalized and analyzed by immunoblotting as described above.

For IHC analysis, FFPE blocks of the tumor and other major organs from the mice were sectioned to 5μm thick and underwent antigen retrieval by incubating in boiling citrate buffer (10 mM Sodium Citrate, 0.05% Tween 20, pH 6.0) for 10min. Sections were then blocked with H_2O_2 and goat serum, followed by staining with hematoxylin/eosin, or with primary antibody overnight in 4°C. Secondary antibody conjugated with HRP was added, followed by DAB substrate for development (2 min). Coloration was quenched with PBS.

Co-immunoprecipitation to study RhoA-GEF and RhoA-GAP interactions

Purified GST-RhoA (10 μg) was immobilized on 15 μL equilibrated glutathione resin (Pierce) and incubated with CL16 in GTP-exchange buffer (20 mM HEPES, 150 mM NaCl, 5 mM $MgCl_2$, pH 7.4) with or without EDTA (1 mM) at room temperature for 1 hour.

Then, the resin was pelleted by centrifugation at 700*g* for 2 min. 120 μg of total cell lysates with overexpression of indicated proteins was added to the resin. After 4 hours incubation with end-to-end rotation at 4°C, the resin was then washed, eluted and subjected to immunoblotting.

RhoA/RhoB/RhoC/Rac1/Cdc42-GTP assay

RhoA-GTP, RhoB-GTP and RhoC-GTP levels were studied by RhoA Activation Assay Biochem Kit (RhoA; Cytoskeleton #BK036), while Rac-1 and Cdc42 levels were studied by Rac1 Pull-Down Activation Assay Biochem Kit (Rac1 and Cdc42; Cytoskeleton #BK035). According to the manufacturer's protocol, total cell lysate (0.5mg/mL; 300 μL) was added to 7.5 μL of corresponding beads and allowed incubation at 4°C for 1 hour. Beads were washed with 500 μL of washing buffer once, centrifuged at 5000*g* for 3 min and the supernatant was discarded. Enriched GTP-bound GTPases were then eluted, resolved and immunoblotted by corresponding Rho GTPase antibodies.

Flow cytometry experiment on cell cycle of CRC cells treated with CL16

HCT116 cells (5 x 10^5 cells), HT29 RhoA WT (1.3 x 10^5 cells) or HT29 RhoA C16A (1.3 x 10^5 cells) pre-attached to 6-well plates were treated with DMSO control or CL16 at the indicated concentration for 24 h. Then, cells were harvested by trypsin digestion, washed with PBS, and fixed in 70% cold ethanol on ice for 30 minutes. The cells were then centrifuged at 250*g* for 5 min and resuspended in staining buffer (PBS with 0.05% Triton X-100) containing propidium iodide (50 μg/mL) and RNase (100 μg/mL) for 30 min at 37°C in the dark. The cells were then filtered through a 40 μm strainer and analyzed by flow cytometry. A representative gating strategy is shown in Data S4. The NovoCyte Advanteon BVYG analyzer was used to acquire cell events, and the data were processed using NovoExpress software.

Apoptosis assay by confocal fluorescence microscopy

HCT116 cells, HT29 RhoA WT or HT29 RhoA C16A were seeded onto a poly-D-lysine coated Ibidi 8-well chamber slide (20,000 cells) and cultured overnight in complete medium at 37°C with 5% CO_2. The cells were co-treated with DMSO control, Rhosin or CL16 with 5 μM of CellEvent™ Caspase-3/7 green in serum-free medium for 24 h. Prior to imaging, the medium was exchanged for HBSS. Confocal fluorescence microscopy was performed using a Zeiss laser scanning microscope 880 with a 20× water-immersion objective lens and ZEN 2.3 (Black Version) software (Carl Zeiss). CellEvent™ Caspase-3/7 green was excited at 488 nm diode laser and emission was collected on a META detector between 490 and 525 nm. Image analysis was performed on ImageJ where the number of cells expressing fluorescence within the field was counted against the total number of cells to report the percentage of apoptotic cells. The average percentage was calculated from 3 separate images from the same well.

Gel-based ABPP to confirm CL16-RhoA engagement

HEK293T cells (3x10^5 cells per well) were plated in a 6-well plate in complete medium and allowed to grow overnight. The cells were transfected with pCMV5-FLAG-RhoA (Addgene #11750) using lipofectamine 2000 according to the manufacturer's protocol, and allowed to grow at 37°C with 5% CO_2 for 48 h. The cells were treated with DMSO or CL16 at indicated concentrations for 2 hours, followed by CL16-alkyne (10 μM) for 2 hours. After treatment, protein lysates were collected. Each sample of 1 mL lysate (1 mg/mL) was pre-cleared by incubation with 50 μL of recombinant Protein G Sepharose (Thermo Scientific, #101241) at 4°C with head-to-head rotation for 2 hours. Sepharose was spun down by centrifugation at 500*g* for 3 min at 4°C. Supernatant was transferred to a new Eppi tube and incubated with 1 μL of anti-FLAG antibody (CST #8146) at 4°C with head-to-head rotation overnight. To enrich FLAG-RhoA, 50 μL of recombinant Protein G Sepharose was added and samples were incubated at 4°C with head-to-head rotation for 4 hours. Samples were centrifuged at 500*g* for 3 min at 4°C, followed by three washes with 500 μL PBS. Sepharose beads were re-suspended in 50 μL PBS for CuAAC. A master-mix solution was added to the beads in PBS, with the final concentrations of azide-fluor 545, copper(II) sulfate, TBTA, and TCEP in the solution mixture at 25 μM, 1 mM, 100 μM and 1 mM, respectively. The beads were incubated in the dark at room temperature with shaking for 1 h. Then, the proteins were eluted by heating the beads with 4× reducing sampling buffer at 90°C for 5 min, separated by SDS-PAGE, and imaged by ChemiDoc MP (Bio-Rad Laboratories, Inc) for measuring in-gel fluorescence. A parallel immunoblotting experiment was performed using anti-FLAG antibody (CST #8146) to confirm the identity of the fluorescent protein band.

LC-MS/MS experiment on HCT116 cells treated with CL16

HCT116 cells were treated with DMSO or CL16 (25 or 50 μM) in complete medium for 4 hours, washed with PBS, harvested, and lysed in PBS by sonication. The protein amount of the samples was determined by BCA assay and normalized. The cell lysates in PBS were reduced by TCEP (1 mM) at 65°C for 30 min, followed by alkylation with iodoacetamide (18 mM) at 37°C for 30 min in the dark. The mixtures were added with prechilled acetone (600 μL) for protein precipitation at -20°C overnight. The samples were centrifuged at 8000*g* for 10 min at 4°C. The supernatant was discarded and the dried pellet was resuspended in 2M urea in PBS (100 μL). Sequencing grade trypsin (Promega #V5111) were added to the samples for overnight digestion at 37°C with constant shaking. The solutions were then acidified with formic acid (FA; final concentration 5%), centrifuged at 13,200 rpm for 30 min at 4°C. The supernatant was collected and stored at -80°C before MS analysis. The peptide solutions were dried and desalted by C18 Stage tips, and the peptides were loaded onto an Aurora C18 UHPLC column (75 μm i.d. × 25 cm length × 1.6 μm particle size (IonOpticks Australia) coupled to timsTOF Pro mass spectrometer (Bruker).

CellPress
OPEN ACCESS

Chromatographic separation by Aurora C18 UHPLC column (75 μm i.d. × 25 cm length × 1.6 μm particle size (IonOpticks Australia) coupled to timsTOF Pro mass spectrometer (Bruker)was carried out using buffer A (98:2 water:acetonitrile, 0.1% formic acid) and B (acetonitrile, 0.1% formic acid) with the gradient from 2% to 30% buffer B at a flow rate of 300 nL/min over 90 min, followed by an increase from 30% to 50% buffer B over 25 min, an isocratic gradient of 95% buffer B over 8.5 min, a decrease of buffer B to 2% in 0.5 min and then an isocratic gradient of 2% buffer B for 5.5 min. MS data was collected over a m/z range of 100 to 1700, and MS/MS range of 100 to 1700. During MS/MS data collection, each TIMS cycle was 1.1 s and included 1 MS + an average of 10 PASEF MS/MS scans.

Raw files were searched using MaxQuant (v2.0.3.0) with Uniprot human database (UP000005640). The search was specified to tryptic digestion (allowed up to 3 cleavages). Cysteine carbamidomethylation (+57.02146) was selected as fixed modification, while N-terminal acetylation (+42.01057), methionine oxidation (+15.99491) and CL16-cysteine adduct (+235.06333) were set as variable modifications. Peptide false discovery rate (FDR) was set to be 1%. Modified peptides with spectral count less than 2, PEP larger than 0.01, and lower spectral counts at 50 μM of CL16 than 25 μM were filtered out.

LC-MS/MS for CL16 target identification using CL16-alkyne

HCT116 cells were treated with DMSO or CL16 (25 μM) in complete medium for 2 hours. The cells were washed with PBS, followed by incubation with CL16-alkyne (50 μM) for 2 hours. After treatment, the cells were washed with PBS and lysed by probe sonication in PBS. Cell debris were removed by centrifugation at 5,000*g* for 10 min at 4°C. After conducting a protein assay using BCA and protein normalization, the cell lysates (4 mg/mL, 2 mL) were mixed with a master-mix solution for CuAAC reaction. The master-mix solution contained $CuSO_4$, TBTA, DTB-PEG-azide, and TECP in final concentrations of 1 mM, 100 μM, 100 μM, and 1 mM respectively. After incubating the samples with the master mix solution for 1 hour at room temperature with vortexing, pre-chilled acetone (12 mL) was added to the samples, and the proteins were allowed to precipitate at -20°C overnight. The samples were centrifuged at 5,000*g* at 4°C for 10 min, and the supernatant was discarded. The protein pellets were then re-dispersed in 1.2% SDS in PBS (w/v) and heated at 80°C for 5 min. Any insoluble solids were discarded by centrifugation at 6,500*g* for 5 min, and the supernatant was transferred to a PBS solution containing Pierce™ Streptavidin Agarose beads (Thermo Scientific #20349) with a final concentration of 0.2% SDS (w/v). The samples and beads were incubated at 4°C with rotation overnight. The beads were then washed with PBS and water, and re-dispersed in 6M urea in PBS. The samples were reduced by TCEP (1 mM) at 65°C for 20 min, followed by alkylation with iodoacetamide (18 mM) at 37°C for 30 min in the dark. The beads were then spun down by centrifugation at 1,400*g* for 2 min, washed with PBS, and re-suspended in 2M urea in PBS. The proteins on the beads were digested by sequencing grade trypsin (Promega) at 37°C overnight. The solution mixtures were then transferred to a BioSpin column (Bio-rad), and the tryptic digested peptides were collected by centrifugation at 1,400*g* for 2 min. The beads were washed with PBS (100 μL) twice. The washing was collected by centrifugation at 1,400*g* for 2 min and combined with the tryptic digested peptide solution. The combined solution was dried and desalted by C18 Stage tips. Finally, the peptides were sent for LC-MS/MS analysis on timsTOF Pro mass spectrometer and analyzed using the aforementioned protocol for the LC-MS/MS experiment. Raw files were searched using MSFragger (v3.7) with Uniprot human database (UP000005640). The search was specified to tryptic digestion (allowed up to 3 cleavages). Cysteine carbamidomethylation (+57.02146) was selected as fixed modification, while N-terminal acetylation (+42.01057) and methionine oxidation (+15.99491) were set as variable modifications. Peptide false discovery rate (FDR) was set to be 1%. For the proteins with zero LFQ intensity for all the 3 replicate runs in the control group and non-zero LFQ intensity for all the 3 runs in the treated group, they were assigned for LFQ ratio of 20. To eliminate false positives, proteins with average intensity smaller than 100,000, combined spectral counts less than 10, or protein probability less than 1 were filtered.

k_{inact}/K_i determination

The binding kinetics between CL16 and RhoA was studied by gel-based experiments using CL16-alkyne as the molecule probe. Briefly, 10 μg of GST-RhoA were pre-immobilized on glutathione resin (Pierce), followed by incubation with CL16 at indicated dosage and duration. The samples were labelled by CL16-alkyne and conjugated to Fluor 545 by CuAAC as in the gel-based ABPP experiment and visualized on SDS-PAGE. In-gel fluorescence intensities from the protein were measured by ImageJ, and the RhoA occupancy by CL16 was determined by:

$$\%\ \text{of RhoA binding by CL16} = (FL_{control} - FL_{CL16}) / FL_{control}$$

where $FL_{control}$ and FL_{CL16} are the in-gel fluorescence intensities from the solvent control and CL16 treatment group respectively.

Experiments were performed in duplicate. Data were plotted and analyzed using GraphPad Prism 9. The k_{obs} values were determined from the initial reactions (slope of the linear region of the % of RhoA binding against time plot) for each CL16 concentration. The k_{obs} values were then plotted against [CL16] and plotted by the previously described double reciprocal method to determine k_{inact}/K_i values.[71]

Assessment of CL16 stability by LC-MS/MS

CL16 (10 μM) was added to corresponding buffer (PBS or PBS with 10% FBS; 100 μL) and incubated for indicated durations. Samples were withdrawn at each time-point and proteins were removed from samples by acetone precipitation. Aqueous supernatants containing CL16 were separated by centrifugation at 13,200 rpm for 10 min, diluted in methanol (1:1000, v/v) and then analysed on LC-MS/MS (SCIEX QTRAP 5500) at the Biomedical Technology Support Centre at the Hong Kong Science Park. Chromatographic

separation was achieved using Waters SunFire C18 Sentry Guard Cartridge (100Å, 5 μm, 4.6 mm X 20 mm) with a gradient of 95% Solvent A (water, 1% formic acid) from 0 min, reaching 100% Solvent B (Acetonitrile, 1% formic acid) at 4 min and lasted till 10 min, returning to 95% Solvent A at 10.5 min and equilibrating till 12 min. Molecular ion with m/z of 329 was selected and the intensity of fragment ion with m/z of 185, determined by the integration of curve, was used for quantification.

QUANTIFICATION AND STATISTICAL ANALYSIS

Figures 2C, 2D, and S2A show results from a single screening experiment. The hit compounds were subsequently confirmed by dose-dependent experiments which were run in triplicate/group (Figures 2E, 2F, and S2B). Unless otherwise specified, all the statistical analyses were performed by two-tailed Student's t-test by MS Excel and all data were expressed as the mean±SD from at least three replicates/group. All of the statistical details of experiments can be found in the figure legends.